Dissociative and Nondissociative Pathways in the *endo* to *exo* Isomerization of Tetramethyl-*o*-xylylene Complexes of Ruthenium and Osmium, $ML_3\{\eta^4\text{-}o\text{-}C_6Me_4(CH_2)_2\}$ (M = Ru, L = PMe_3; M = Os, L = PMe_3, PMe_2Ph). Formation of Hexamethylbenzene-1,2-diyl Complexes by Ligand Addition to the *exo*-Osmium Complexes

Martin A. Bennett,*,† Mark Bown,† David C. R. Hockless,† John E. McGrady,‡ Harold W. Schranz,† Robert Stranger,‡ and Anthony C. Willis†

Research School of Chemistry and the Department of Chemistry, Australian National University, Canberra, ACT 0200, Australia

Received May 26, 1998

Treatment of the (η^6-hexamethylbenzene)ruthenium(II) and -osmium(II) salts $[M(O_2CCF_3)L_2(\eta^6\text{-}C_6Me_6)]PF_6$ (M = Ru, L = PMe_3; M = Os, L = PMe_3, PMe_2Ph) in the presence of L with KO-*t*-Bu gives exclusively the *endo*- *(*tetramethyl-*o*-xylylene)metal(0) complexes $ML_3\{\eta^4\text{-}endo\text{-}o\text{-}C_6Me_4(CH_2)_2\}$, *endo*-**1**, -**2**, and -**3**, respectively, in high yield; these are protonated by an excess of triflic acid (CF_3SO_3H, TfOH) to give the (η^6-hexamethylbenzene)metal(II) salts $[ML_3(\eta^6\text{-}C_6Me_6)](OTf)_2$ [M = Ru, L = PMe_3 (**4**); M = Os, L = PMe_3 (**5**); M = Os, L = PMe_2Ph (**6**)). Complexes **4**−**6** revert to *endo*-**1**−**3** on treatment with KO-*t*-Bu, whereas for M=Ru, L=PMe_2Ph the complexes $[ML_3(\eta^6\text{-}C_6Me_6)]^{2+}$ and $[M(O_2CCF_3)L_2(\eta^6\text{-}C_6Me_6)]^+$/L react with KO-*t*-Bu to give exclusively the *exo* isomer, $Ru(PMe_2Ph)_3\{\eta^4\text{-}exo\text{-}o\text{-}(CH_2)_2C_6Me_4\}$ (*exo*-**7**). The *endo* complexes **1**−**3** are converted quantitatively into the corresponding *exo* isomers in toluene in the temperature range 65−106 °C, the process being first order in *endo* complex. Kinetics studies in the presence of PMe_3 (for **1** and **2**) or PMe_2Ph (for **3**) indicate that two pathways are available: one depends on initial dissociation of L and proceeds through a bis(ligand) intermediate or intermediates, e.g., $ML_2\{endo\text{-}o\text{-}C_6Me_4(CH_2)_2\}$ and $ML_2\{exo\text{-}o\text{-}(CH_2)_2C_6Me_4\}$, and the other does not. The dissociative mechanism is predominant for M = Ru, L = PMe_3, whereas the nondissociative or direct mechanism plays the dominant, possibly exclusive, role for M = Os, L = PMe_3. The osmium(0) compound *exo*-**2** adds PMe_3 irreversibly to give the σ-bonded (hexamethylbenzene-1,2-diyl)osmium(II) complex $Os(PMe_3)_4\{\kappa^2\text{-}o\text{-}(CH_2)_2C_6Me_4\}$ (**8**), whereas the corresponding PMe_2Ph derivative **9** is in equilibrium with *exo*-**3** and PMe_2Ph and cannot be isolated; the ruthenium(0) compound *exo*-**1** is inert toward PMe_3. Density functional calculations on the model compounds $ML_3\{\eta^4\text{-}exo\text{-}o\text{-}(CH_2)_2C_6H_4\}$ and $ML_4\{\kappa^2\text{-}o\text{-}(CH_2)_2C_6H_4\}$(M = Ru, Os; L = PH_3) correctly reflect the observed stability order Os > Ru for the diyl complex but predict the latter to be more stable than the η^4 complex for both elements. In this case, the usual computational simplification of replacing a tertiary phosphine by PH_3 is probably unjustified. The molecular structures of the η^4 complexes *endo*-**3**, *exo*-**3**, and *exo*-**1** and of the diyl complex **8** have been determined by X-ray crystallography. The *endo*- to *exo*-*o*-xylylene isomerizations are compared with the intramolecular migrations that occur in $Fe(CO)_3(\eta^4$-polyene) and $Cr(CO)_3(\eta^6$-substituted-naphthalene) complexes.

Introduction

In its mononuclear complexes, *o*-xylylene (*o*-quinodimethane, xylene-1,2-diyl) can bind as a η^4 conjugated diene to transition-metal atoms either via the endocyclic pair of double bonds (Figure 1a), as in $M(\eta^6\text{-}C_6Me_6)\{\eta^4\text{-}o\text{-}C_6Me_4(CH_2)_2\}$ (M = Fe,[1,2] Ru[3,4]), or via the exocyclic pair of double bonds (Figure 1b), as in $Fe(CO)_3\{\eta^4\text{-}o\text{-}(CH_2)_2C_6H_4\}$[5,6] and $Co(\eta^5\text{-}C_5H_5)\{\eta^4\text{-}o\text{-}(CH_2)_2C_6H_4\}$.[7] As

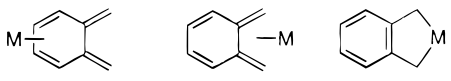

Figure 1. Coordination modes for *o*-xylylene.

† Research School of Chemistry.
‡ Department of Chemistry.

(1) Madonic, A. M.; Astruc, D. *J. Am. Chem. Soc.* **1984**, *106*, 2437.
(2) Astruc, D.; Mandon, D.; Madonik, A.; Michaud, P.; Ardoin, N.; Varret, F. *Organometallics* **1990**, *9*, 2155.
(3) Hull, J. W., Jr.; Mann, C.; Gladfelter, W. L. *Organometallics* **1992**, *11*, 3117.
(4) Hull, J. W., Jr.; Gladfelter, W. L. *Organometallics* **1982**, *1*, 1716.

S0276-7333(98)00422-1 CCC: $15.00
Publication on Web 07/21/1998

shown in Figure 1c, *o*-xylylene can also behave as a two-electron *σ*-donor ligand via the exocyclic methylene groups, mainly to metal atoms in medium to high oxidation states; examples of mononuclear κ^2 complexes of this type are Pt{*o*-$(CH_2)_2C_6H_4$}(1,5-COD),[8] M(η^5-$C_5H_5)_2\{\eta^4$-*o*-$(CH_2)_2C_6H_4\}$ (M = Ti, Zr, Hf),[9] and W{η^4-*o*-$(CH_2)_2C_6H_4\}_3$.[10]

We have shown that the $4d^8$ fragment $Ru(PMe_2Ph)_3$ is capable of coordinating *o*-xylylene in both *exo* and *endo* modes. Deprotonation of the (arene)ruthenium(II) monocationic salts $[Ru(O_2CCF_3)(PMe_2Ph)_2(\eta^6$-arene$)]PF_6$ (arene = C_6Me_6, 1,2-$C_6H_4Me_2$) with KO-*t*-Bu or $Na[N(SiMe_3)_2]$ in the presence of PMe_2Ph gives the corresponding *exo*-*o*-xylylene complexes (eq 1),[11] whereas

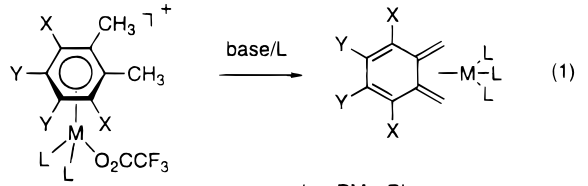

(1)

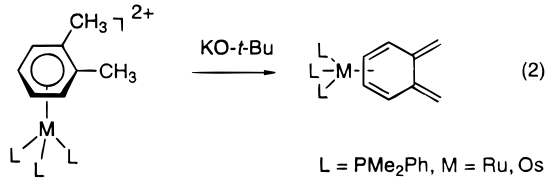

(2)

treatment of the dicationic salts [M(η^6-*o*-$C_6H_4Me_2$)($PMe_2Ph)_3](PF_6)_2$ (M = Ru, Os) with KO-*t*-Bu gives exclusively the *endo*-*o*-xylylene complexes $M(PMe_2Ph)_3\{\eta^4$-*o*-$(CH_2)_2C_6H_4\}$ (eq 2).[12] The *exo* complexes have also been made independently by reaction of $RuCl_2(PMe_2Ph)_4$ with the appropriate *o*-methylbenzyl Grignard or lithium reagents.[13−15] Density functional calculations on the model compound $Ru(PH_3)_3\{\eta^4$-*o*-$(CH_2)_2C_6H_4\}$ show that the *exo* compound is ca. 60 kJ mol^{-1} more stable than its *endo* isomer, mainly because of aromatic stabilization in the former;[16] however, since no thermal interconversion of the isomers was observed, it was assumed that the process must be thermally forbidden. In this report, we extend our studies to tetramethyl-*o*-xylylene complexes of ruthenium with PMe_3 as coligand and of osmium with PMe_3 and PMe_2Ph as coligands and show that in these compounds thermal isomerization occurs much more easily; further, for osmium with PMe_2Ph, the η^4-*exo* and κ^2 bonding modes are interconvertible.

Experimental Section

General Procedures. The following instruments were used: Varian XL200 (^{13}C NMR at 50.29 MHz), Varian VXR-300S and Varian Gemini 300 (^1H NMR at 300 MHz, ^{31}P NMR at 121.42 MHz, ^{13}C NMR at 75.43 MHz), Varian VXR-500S (^1H NMR at 500 MHz), VG AutoSpec (EI mass spectra at 70 eV) and VG ZAB-2SEQ (EI at 70 eV, FAB at 30 kV, Cs ions using a NBA matrix), VG Quattro II (electrospray triple quadrupole), and Perkin-Elmer 683 (infrared). The NMR spectroscopic data for the tetramethyl-*o*-xylylene complexes are collected in Tables 1 and 2.

Organic solvents of reagent grade were dried by published procedures[17] and distilled under nitrogen before use. All operations with *endo*- and *exo*-tetramethyl-*o*-xylylene complexes were carried out under argon by standard Schlenk techniques. The (η^6-hexamethylbenzene)-ruthenium(II) and -osmium(II) precursors were handled in air. Elemental analyses were carried out in-house. The compounds $[Ru(O_2CMe)_2(\eta^6$-$C_6Me_6)]\cdot H_2O$,[18] $[OsCl_2(\eta^6$-$C_6Me_6)]_2$,[19,20] and $[Ru(PMe_2Ph)_3(C_6Me_6)](CF_3SO_3)_2$[11] were prepared as described.

Preparations. (a) $Ru(O_2CCF_3)_2(PMe_3)(\eta^6$-$C_6Me_6)$. This compound has been prepared previously by treatment of $RuMe_2(PMe_3)(\eta^6$-$C_6Me_6)$ with an excess of CF_3CO_2H.[21] We made it as follows. A sample of $[Ru(O_2CMe)_2(\eta^6$-$C_6Me_6)]\cdot H_2O$ (200 mg, 0.501 mmol) was treated with trifluoroacetic acid (4 mL) at room temperature for 4 h. The excess acid was removed under reduced pressure and the orange crystalline product, presumed to be $[Ru(O_2CCF_3)_2(\eta^6$-$C_6Me_6)]$, was dissolved in dichloromethane (10 mL) to give a yellow-orange solution. Addition of PMe_3 (52 μL, 0.502 mmol) gave an orange solution, which was stirred at room temperature for 17 h. The solvent was removed under reduced pressure, and the residue was washed with *n*-hexane (3 × 20 mL). Yellow microcrystals of $Ru(O_2CCF_3)_2(PMe_3)(\eta^6$-$C_6Me_6)$ (257 mg, 92%) were obtained by crystallization from dichloromethane/*n*-hexane. ^1H NMR (CD_2Cl_2, 300 MHz): δ 2.08 (d, J_{PH} = 1.0 Hz, C_6Me_6), 1.33 (d, J_{PH} = 10.8 Hz, PMe_3). Lit.[21] ^1H NMR (C_6H_6, 60 MHz): δ 1.69 (d, J_{PH} = 0.8 Hz, C_6Me_6), 1.06 (d, J_{PH} = 8.3 Hz, PMe_3). $^{31}P\{^1H\}$ NMR (CD_2Cl_2, 121.42 MHz): δ 6.30. Lit.[21] $^{31}P\{^1H\}$ NMR (C_6H_6, 36.43 MHz): δ 3.64. $^{13}C\{^1H\}$ NMR (CD_2Cl_2, 75.43 MHz): δ 95.09 (s, C_6Me_6), 16.37 (s, C_6Me_6), 13.87 (d, J_{PC} = 29.65 Hz, PMe_3).

This compound was converted into $[Ru(O_2CCF_3)(PMe_3)_2(\eta^6$-$C_6Me_6)]PF_6$ by treatment with PMe_3/NH_4PF_6.[21]

(b) $Os(O_2CCF_3)_2(PMe_3)(\eta^6$-$C_6Me_6)$. A mixture of $[OsCl_2(\eta^6$-$C_6Me_6)]_2$ (100 mg, 0.181 mmol) and silver acetate (85 mg, 0.50 mmol) was stirred for 12 h in benzene (20 mL). The resulting solution was filtered through Celite to remove AgCl, solvent was removed under reduced pressure, and the solid yellow residue was treated with trifluoroacetic acid (4 mL) for 30 min to give a blue solution (the color probably arises from traces of osmium trifluoroacetato complexes formed by loss of arene). The excess of acid was removed under reduced pressure, and the residue was dissolved in dichloromethane (10 mL) to give a deep blue solution. Addition of PMe_3 (40 μL, 0.386 mmol)

(5) Roth, W. R.; Meier, J. D. *Tetrahedron Lett.* **1967**, 2053.
(6) Johnson, B. F. G.; Lewis, J.; Thompson, D. J. *Tetrahedron Lett.* **1974**, 3789.
(7) Hersh, W. H.; Hollander, F. J.; Bergman, R. G. *J. Am. Chem. Soc.* **1983**, *105*, 5834.
(8) Lappert, M. F.; Martin, T. R.; Raston, C. L.; Skelton, B. W.; White, A. H. *J. Chem. Soc., Dalton Trans.* **1982**, 1959.
(9) Bristow, G. S.; Lappert, M. F.; Martin, T. R.; Atwood, J. L.; Hunter, W. F. *J. Chem. Soc., Dalton Trans.* **1984**, 399.
(10) Lappert, M. F.; Raston, C. L.; Rowbottom, G. L.; Skelton, B. W.; White, A. H. *J. Chem. Soc., Dalton Trans.* **1984**, 883.
(11) Bennett, M. A.; Goh, L. Y.; McMahon, I. J.; Mitchell, T. R. B.; Robertson, G. B.; Turney, T. W.; Wickramasinghe, W. A. *Organometallics* **1992**, *11*, 3069.
(12) Bennett, M. A.; Bown, M.; Goh, L. Y.; Hockless, D. C. R.; Mitchell, T. R. B. *Organometallics* **1995**, *14*, 1000.
(13) Chappell, S. D.; Cole-Hamilton, D. J.; Galas, A. M. R.; Hursthouse, M. B. *J. Chem. Soc., Dalton Trans.* **1982**, 1867.
(14) Simpson, N. J.; Cole-Hamilton, D. J. *Polyhedron* **1988**, *19/20*, 1945.
(15) Simpson, N. J.; Cole-Hamilton, D. J. *J. Chem. Soc., Dalton Trans.* **1990**, 1329.
(16) McGrady, J. E.; Stranger, R.; Bown, M.; Bennett, M. A. *Organometallics* **1996**, *15*, 3109.
(17) Perrin, D. D.; Armarego, W. L. F. *Purification of Laboratory Chemicals*, 4th ed.; Butterworth-Heinemann: Oxford, U.K., 1996.
(18) Tocher, D. A.; Gould, R. O.; Stephenson, T. A.; Bennett, M. A.; Ennett, J. P.; Matheson, T. W.; Sawyer, L. S.; Shah, V. K. *J. Chem. Soc., Dalton Trans.* **1983**, 1571.
(19) Bown, M.; Fontaine, X. L. R.; Greenwood, N. N.; Kennedy, J. D. *J. Organomet. Chem.* **1987**, *325*, 233.
(20) Kiel, W. A.; Ball, R. G.; Graham, W. A. G. *J. Organomet. Chem.* **1990**, *383*, 481.
(21) Werner, H.; Kletzin, H. *J. Organomet. Chem.* **1982**, *228*, 289.

Table 1. ^{1}H, ^{13}C{^{1}H}, and ^{31}P{^{1}H} NMR Data for *o*-Xylylene Compounds *endo*-1−3 and *exo*-1−3[a,b]

		o-xylylene		phosphine		
	assgt	$\delta(^{13}C\{^{1}H\})$	$\delta(^{1}H)$	$\delta(^{31}P\{^{1}H\})$	$\delta(^{1}H)$	$\delta(^{13}C)$
$Ru(PMe_3)_3\{\eta^4$-*endo*-*o*-$C_6Me_4(CH_2)_2\}$[c] (**1**)	$=CH_2$	90.74	4.57 (m), 5.29 (m)	−4.6 (d, 2P)	P*Me*$_3$: 1.25 (dd, 9H, J_{PH} = 1.1, 6.9 Hz), 0.97 (m, 18H)	P*Me*$_3$: 25.04 (appt td, 6C, 3.3,11.0 Hz), 19.33 (d, 3C, 20.9 Hz)
	$C_{1,2}$	154.16 (d, J_{PC} = 4.4 Hz)		−12.8 (t, 1P, J_{PP} = 11.5 Hz)		
	$C_{3,6}$	25.03 (td, J_{PC} = 3.3, 10.7 Hz)				
	$C_{4,5}$	80.30 (d, J_{PC} = 3.3 Hz)				
	$H-C_{31,61}$	22.86	1.71 (m)			
	$H-C_{41,51}$	17.87	1.90 (m)			
$Os(PMe_3)_3\{\eta^4$-*endo*-*o*-$C_6Me_4(CH_2)_2\}$][d,e] (**2**)	$=CH_2$	92.10	4.53 (m), 5.28 (m)	−54.2 (d, 2P)	P*Me*$_3$: 1.37 (dd, 9H, J_{PH} = 1.0, 8.0 Hz), 1.15 (dd, 18H, J_{PH} = 1.0, 6.6 Hz)	P*Me*$_3$: 25.56 (sym m, 6C), 20.35 (appt dt, 3C, 29.0, 2.1 Hz)
	$C_{1,2}$	156.02 (d, J_{PC} = 4.2 Hz)		−55.1 (t, 1P, J_{PP} = 6.1 Hz)		
	$C_{3,6}$	47.97 (td, J_{PC} = 4.6, 12.5 Hz)				
	$C_{4,5}$	86.04 (dt, J_{PC} = 5.0, 2.1 Hz)				
	$H-C_{31,61}$	23.53	1.71 (d, J_{PH} = 3.6 Hz)			
	$H-C_{41,51}$	17.39	2.00 (dt, J_{PH} = 2.4, 0.7 Hz)			
$Os(PMe_2Ph)_3\{\eta^4$-*endo*-*o*-$C_6Me_4(CH_2)_2\}$[f−h] (**3**)	$=CH_2$	94.70	4.43 (s), 5.29 (s)	−36.6 (d, 2P)	P*Me*$_2$Ph: 1.91 (d, 6H, J_{PH} = 7.9 Hz), 1.57 (d, 6H, J_{PH} = 6.9 Hz), 1.27 (d, 6H, J_{PH} = 6.4 Hz)	P*Me*$_2$Ph: 23.60 (d, 2C, 1.6 Hz), 23.32 (m, 2C), 19.47 (m, 2C)
	$C_{1,2}$	155.29 (d, J_{PC} = 4.1 Hz)		−39.1 (t, 1P, J_{PP} = 8.7 Hz)		
	$C_{3,6}$	46.96 (td, J_{PC} = 4.6, 12.8 Hz)				
	$C_{4,5}$	86.96 (d, J_{PC} = 5.2 Hz)			PMe$_2$*Ph*: 6.9−7.7 (m, 15H)	PMe$_2$*Ph*: 125−147 (m)
	$H-C_{31,61}$	23.11	1.38 (t, J_{PH} = 3.4 Hz)			
	$H-C_{41,51}$	15.59 (d, J_{PC} = 1.9 Hz)	1.59 (d, J_{PH} = 2.4 Hz)			
$Ru(PMe_3)_3\{\eta^4$-*exo*-*o*-$(CH_2)_2C_6Me_4\}$[d,f,i] (**1**)	$=CH_2$	27.61 (m)	−0.38 (m, H_{anti}), 2.09 (m, H_{syn})	−7.4 (d, 2P)	P*Me*$_3$: 1.35 (d, 9H, J_{PH} = 7.8 Hz), 0.91 (vt, 18H, $^{2}J_{PH}$ + $^{4}J_{PH}$ = 5.7 Hz)	P*Me*$_3$: 23.37 (appt t, 6C, 10.4 Hz), 25.26 (appt dt, 3C, 23.3, 2.9 Hz)
	$C_{1,2}$	102.3 (q, J_{PC} = 2.2 Hz)		14.5 (t, 1P, J_{PP} = 7.3 Hz)		
	$C_{3,6}$	132.82				
	$C_{4,5}$	132.03				
	$H-C_{31,61}$	18.40	2.36 (s)			
	$H-C_{41,51}$	17.66	2.13 (s)			
$Os(PMe_3)_3\{\eta^4$-*exo*-*o*-$(CH_2)_2C_6Me_4\}$[j] (**2**)	$=CH_2$	22.40 (m)	−0.02 (m, H_{anti}), 2.50 (m, H_{syn})	−55.0 (d, 2P)	P*Me*$_3$: 1.50 (d, 9H, J_{PH} = 8.8 Hz), 1.08 (d, 18H, J_{PH} = 6.5 Hz)	P*Me*$_3$: 24.09 (appt td, 6C, 15.4, 3.9 Hz), 25.51 (appt dt, 3C, 31.3, 3.0 Hz)
	$C_{1,2}$	97.86 (q, J_{PC} = 2.6 Hz)		−38.0 (t, 1P, J_{PP} = 11.5 Hz)		
	$C_{3,6}$	132.57				
	$C_{4,5}$	130.07				
	$H-C_{31,61}$	19.10	2.14 (s)			
	$H-C_{41,51}$	17.38	2.41 (s)			
$Os(PMe_2Ph)_3\{\eta^4$-*exo*-*o*-$(CH_2)_2C_6Me_4\}$[f,h] (**3**)	$=CH_2$	22.99 (m)	−0.06 (m, H_{anti}), 2.51 (m, H_{syn})	−39.7 (d, 2P)	P*Me*$_2$Ph: 1.89 (d, 6H, J_{PH} = 8.6 Hz), 1.33 (d, 6H, J_{PH} = 6.4 Hz), 1.26 (d, 6H, J_{PH} = 6.1 Hz)	P*Me*$_2$Ph: 23.38 (appt dt, 3C, 32.63, 2.3 Hz), 22.67 (d, 3C, 12.2 Hz), 22.46 (d, 3C, 11.2 Hz)
	$C_{1,2}$	99.54 (q, J_{PC} = 2.3 Hz)		−26.6 (t, 1P, J_{PP} = 14.8 Hz)		
	$C_{3,6}$	132.82				
	$C_{4,5}$	132.03			PMe$_2$*Ph*: 6.5−7.6 (m, 15H)	PMe$_2$*Ph*: 126−147 (m)
	$H-C_{31,61}$	18.40	2.09 (s)			
	$H-C_{41,51}$	17.66	2.14 (s)			

[a] Numbering of *o*-xylylene nuclei:

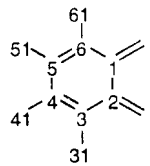

[b] ^{1}H NMR at 300 MHz, ^{31}P NMR at 121.42 MHz, and ^{13}C NMR at 75.43 MHz in benzene-d_6 at 298 K, except where stated otherwise. [c] ^{1}H and ^{13}C resonances were assigned by comparison with the spectra of *endo*-**3** and *endo*-**2**. [d] ^{1}H NMR at 500 MHz. [e] Assignments of ^{1}H and ^{13}C resonances were obtained from multiple-bond 2D [^{1}H−^{13}C]-GHMQC experiments at 500 MHz. [f] In toluene-d_8 at 298 K. [g] ^{13}C NMR at 50.29 MHz. [h] ^{1}H and ^{13}C resonances were assigned from single- and multiple-bond 2D [^{1}H−^{13}C]-GHMQC experiments at 500 MHz. [i] ^{1}H and ^{13}C resonances were assigned from a multiple-bond 2D [^{1}H-^{13}C]-GHMQC experiment at 500 MHz and a [^{1}H−^{13}C] COSY experiment at 75.43 MHz. [j] ^{1}H and ^{13}C resonances were assigned by comparison with the spectra of *exo*-**3**.

Table 2. ^{1}H, ^{13}C{^{1}H}, and ^{31}P{^{1}H} NMR Data for κ^2-*o*-Xylylene Compounds 8 and 9[a,b]

		o-xylylene		phosphine[e]	
	assgt	δ(^{13}C{^{1}H})	δ(^{1}H)	δ(^{31}P{^{1}H})	δ(^{1}H)
Os(PMe$_3$)$_4${κ^2-*o*-(CH$_2$)$_2$-C$_6$Me$_4$}[c] (**8**)	=CH$_2$	9.37 [dtd, J(PC) = 48.5, 9.1, 4.8 Hz]	2.38 [tt, J(P$_A$H) = 12.6 Hz, J(P$_B$H) = 5.4 Hz]	−47.6 [t, 2P$_A$]	P$_A$Me$_3$: 1.30 [d, J(PH) = 5.7 Hz]
	C$_{1,2}$	153.09 [dt, J(PC) = 10.4, 4.5 Hz]		−58.4 [t, 2P$_B$, J(PP) = 16.5 Hz]	P$_B$Me$_3$: 1.04 [t, J(PH) = 2.9 Hz]
	C$_{3,6}$	131.46			
	C$_{4,5}$	128.60			
	H−C$_{31,61}$	16.74	2.58 (s)		
	H−C$_{41,51}$	16.92	2.28 (s)		
Os(PMe$_2$Ph)$_4${κ^2-*o*-(CH$_2$)$_2$-C$_6$Me$_4$}[d] (**9**)	=CH$_2$	9.11 [t, J(PC) = 16.47 Hz]	2.27 [tt, J(PH) = 11.2, 5.5 Hz]	−35.4 [t, 2P]	PMe$_2$Ph: 1.65 [d, 12H, J(PH) = 4.6 Hz], 1.10 [vt, 12H, ^2J(PH) + ^4J(PH) = 4.5 Hz].
	C$_{1,2}$	153.24 [dt, J(PC) = 9.8, 5.5 Hz]		−47.9 [t, 2P, J(PP) = 13.1 Hz]	
	C$_{3,6}$	130.94			PMe$_2$*Ph*: 6.75 − 7.60(m, 20H)
	C$_{4,5}$	128.04			
	H−C$_{31,61}$	16.60	2.39 (s)		
	H−C$_{41,51}$	16.88	2.34 (s)		

[a] *o*-Xylylene nuclei numbered as in Table 1. [b] In toluene-d_8 at 298 K; measuring frequencies as in Table 1. [c] ^{1}H and ^{13}C resonances were assigned from a multiple-bond 2D [^{1}H−^{13}C]-GHMQC experiment at 500 MHz and a [^{1}H−^{13}C] COSY experiment at 75.43 MHz. [d] ^{1}H and ^{13}C resonances were assigned by comparison with the spectra of **8**. [e] ^{13}C NMR for PMe$_3$ ligands in **8**: δ 18.78 (app tt, sepn 14.3, 2.5 Hz), 16.60 (app dd, sepn = 34.2, 13.9 Hz). ^{13}C NMR for PMe$_2$Ph ligands in **9**: δ 131−127 (m, Ph), 17.4−15.4 (m, Me).

gave an orange solution, which was stirred at room temperature for 1 h. The solvent was removed under reduced pressure and the residue washed with *n*-hexane (3 × 20 mL). Yellow microcrystals of Os(O$_2$CCF$_3$)$_2$(PMe$_3$)(η^6-C$_6$Me$_6$) (175 mg, 74%) were obtained by crystallization from dichloromethane/*n*-hexane. ^{1}H NMR (CD$_2$Cl$_2$, 300 MHz): δ 2.11 (s, C$_6$Me$_6$), 1.36 (d, $^2J_{PH}$ = 10.5 Hz, PMe$_3$). ^{31}P{^{1}H} NMR (CD$_2$Cl$_2$, 121.42 MHz): δ 30.35 (s). MS (FAB): *m*/*z* 656, [M]$^+$. Anal. Calcd for C$_{19}$H$_{27}$F$_6$O$_4$OsP: C, 34.86; H, 4.16. Found: C, 34.83; H, 4.05.

(c) [Os(O$_2$CCF$_3$)(PMe$_3$)$_2$(η^6-C$_6$Me$_6$)]PF$_6$. A sample of [Os(O$_2$CCF$_3$)$_2$(PMe$_3$)(η^6-C$_6$Me$_6$)] in methanol (5 mL), which had been made directly, without isolation, from [OsCl$_2$(η^6-C$_6$Me$_6$)]$_2$ (249 mg, 0.293 mmol), was treated successively with PMe$_3$ (125 μL, 1.23 mmol) and NH$_4$PF$_6$ (1.65 g, 10.12 mmol) in water (1.5 mL) to give the product as a pale yellow precipitate. After filtration, washing with water, and drying under vacuum, 323 mg (72%) of the product was obtained. ^{1}H NMR (CD$_2$Cl$_2$, 300 MHz): δ 2.20 (s, C$_6$Me$_6$), 1.59 (vt, $^2J_{PH} + {}^4J_{PH}$ = 10.0 Hz, PMe$_3$). ^{31}P{^{1}H} NMR (CD$_2$Cl$_2$, 121.42 MHz) δ −40.7 (s, PMe$_3$), −143.8 (spt, PF$_6$, J_{PF} = 711 Hz). MS (FAB): *m*/*z* 619, [M − PF$_6$]$^+$. Anal. Calcd for C$_{20}$H$_{36}$F$_9$O$_2$OsP$_3$: C, 31.50; H, 4.76; P, 12.18. Found: C, 31.03; H, 4.75; P, 12.08.

(d) [Os(O$_2$CCF$_3$)(PMe$_2$Ph)$_2$(η^6-C$_6$Me$_6$)]PF$_6$. A mixture of [OsCl$_2$(η^6-C$_6$Me$_6$)]$_2$ (213 mg, 0.252 mmol) and silver acetate (168 mg, 1.01 mmol) was stirred for 69 h in benzene (50 mL) and treated with trifluoroacetic acid (4 mL) as described in (b). The blue residue obtained after removal of the excess acid was dissolved in methanol (10 mL) to give a red−blue dichroic solution. Successive addition of PMe$_2$Ph (142 μL, 1.00 mmol) and a solution of NH$_4$PF$_6$ (600 mg) in water (500 μL) precipitated the required compound as a yellow solid (175 mg), which was collected by filtration, washed with water, and dried in vacuo. The mother liquor was evaporated to dryness under reduced pressure. The residue was washed with water and extracted with dichloromethane (ca. 10 mL). The filtered extract was concentrated under reduced pressure to ca. 2 mL. Addition of ether gave a second crop of product (176 mg) as a crystalline yellow solid. The total amount of [Os(O$_2$CCF$_3$)(PMe$_2$Ph)$_2$(η^6-C$_6$Me$_6$)]PF$_6$ was 351 mg (79%). ^{1}H NMR (CD$_2$Cl$_2$, 300 MHz): δ 7.7−7.4 (m, PMe$_2$*Ph*), 1.83 (s, C$_6$Me$_6$), 1.81 (vt, $^2J_{PH} + {}^4J_{PH}$ = 9.3 Hz), 1.63 (vt, $^2J_{PH} + {}^4J_{PH}$ = 10.2 Hz) (P*Me*$_2$Ph). ^{31}P{^{1}H} NMR (CD$_2$Cl$_2$, 121.42 MHz): δ −35.7 (s, PMe$_2$Ph), −143.8 (spt, PF$_6$, J_{PF} = 711 Hz). MS (FAB): *m*/*z* 743, [M − PF$_6$]$^+$. Anal. Calcd for C$_{30}$H$_{40}$F$_9$O$_2$OsP$_3$: C, 40.63; H, 4.55. Found: C, 40.46; H, 4.35.

(e) Ru(PMe$_3$)$_3${η^4-*endo*-*o*-C$_6$Me$_4$(CH$_2$)$_2$}, *endo*-1. A stirred suspension of [Ru(O$_2$CCF$_3$)(PMe$_3$)$_2$(η^6-C$_6$Me$_6$)]PF$_6$ (176 mg, 0.26 mmol) in THF (30 mL) was treated successively with PMe$_3$ (27 μL, 0.265 mmol) and an excess of KO-*t*-Bu (293 mg, 2.6 mmol), and the mixture was stirred at room temperature for 18 h. The THF was removed under reduced presure, and the yellow residue was extracted with ether (2 × 20 mL). The solution was filtered through Celite, and the solvent was removed under reduced pressure to give *endo*-**1** as a yellow, crystalline solid (112 mg, 88%). IR (KBr disk): 1510 cm^{-1} (ν-(free C═C)). MS (EI): *m*/*z* 490 (parent ion). Anal. Calcd for C$_{21}$H$_{43}$RuP$_3$: C, 51.52; H, 8.85. Found: C, 51.23; H, 8.85.

(f) Ru(PMe$_3$)$_3${η^4-*o*-*exo*-(CH$_2$)$_2$C$_6$Me$_4$}, *exo*-1. A sample of *endo*-**1** (ca. 30 mg) in toluene-d_8 (ca. 600 μL) was heated at 110 °C for 16 h, during which time the solution changed from yellow to deep gold. Monitoring by ^{1}H and ^{31}P{^{1}H} NMR spectroscopy showed the *endo* to *exo* isomerization was quantitative and complete. The solvent was removed under reduced pressure to give *exo*-**1** as yellow crystals. X-ray-quality crystals were grown by slow evaporation of the toluene-d_8 solution. MS (EI): *m*/*z* 490 (parent ion). Anal. Calcd for C$_{21}$H$_{43}$RuP$_3$: C, 51.52; H, 8.85. Found: C, 51.25; H, 8.62.

(g) Os(PMe$_3$)$_3${η^4-*endo*-*o*-C$_6$Me$_4$(CH$_2$)$_2$}, *endo*-2. This was obtained as a yellow, crystalline solid similarly to *endo*-**1** from [Os(O$_2$CCF$_3$)(PMe$_3$)$_2$(η^6-C$_6$Me$_6$)]PF$_6$ (312 mg, 0.41 mmol) in

THF (40 mL), PMe_3 (41 μL, 0.40 mmol), and an excess of KO-*t*-Bu (449 mg, 4.0 mmol). The yield was 228 mg (96%). IR (KBr disk): 1572 cm^{-1} (ν(free C=C)). MS (EI): *m*/*z* (parent ion) calcd for $^{12}C_{21}{}^{1}H_{43}{}^{192}Os^{31}P_3$ 580.2193, found 580.2179. Anal. Calcd for $C_{21}H_{43}OsP_3$: C, 43.59; H, 7.49; P, 16.06. Found: C, 43.01; H, 8.02; P, 15.82.

(h) Os(PMe$_3$)$_3${η^4-*exo*-*o*-(CH$_2$)$_2$C$_6$Me$_4$}, *exo*-2. This was prepared as yellow microcrystals from *endo*-**2** by following the procedure for *exo*-**1**. MS (EI): *m*/*z* (parent ion) calcd for $^{12}C_{21}{}^{1}H_{43}{}^{192}Os^{31}P_3$ 580.2193, found 580.2179. Anal. Calcd for $C_{21}H_{43}OsP_3$: C, 43.59; H, 7.49. Found: C, 43.72; H, 7.32.

(i) Os(PMe$_2$Ph)$_3${η^4-*endo*-*o*-C$_6$Me$_4$(CH$_2$)$_2$}, *endo*-3. This was obtained as a yellow solid similarly to *endo*-**1** from [Os(O$_2$CCF$_3$)(PMe$_2$Ph)$_2$(η^6-C$_6$Me$_6$)]PF$_6$ (173 mg, 0.195 mmol) in THF (40 mL), PMe_2Ph (28μL, 0.197 mmol), and an excess of KO-*t*-Bu (66 mg, 0.585 mmol), the mixture being stirred at room temperature for 24 h. The yield was 125 mg (84%). X-ray-quality crystals were grown by diffusion of pentane into a benzene solution. IR (KBr disk): 1584 cm^{-1} (ν(free C=C)). MS (EI): *m*/*z* (parent ion) calcd for $^{12}C_{36}{}^{1}H_{49}{}^{192}Os^{31}P_3$ 766.2662, found 766.2664. Anal. Calcd for $C_{36}H_{49}P_3Os$: C, 56.53; H, 6.46. Found: C, 56.43; H, 6.42.

(j) Os(PMe$_2$Ph)$_3${η^4-*exo*-*o*-(CH$_2$)$_2$C$_6$Me$_4$}, *exo*-3. This was obtained similarly to *exo*-**1** by heating *endo*-**3** in toluene-d_8 at 70 °C for 16 h. X-ray-quality crystals were grown from isopentane at −78 °C. MS (EI): *m*/*z* (parent ion) calcd for $^{12}C_{36}{}^{1}H_{49}{}^{192}Os^{31}P_3$ 766.2662, found 766.2656. Anal. Calcd for $C_{36}H_{49}OsP_3$: C, 56.53; H, 6.46. Found: C, 55.80; H, 6.51.

(k) [Ru(PMe$_3$)$_3$(η^6-C$_6$Me$_6$)](CF$_3$SO$_3$)$_2$ (4). (i) A solution of *endo*-**1** (71 mg, 0.145 mmol) in THF (20 mL) was treated with an excess of triflic acid (130 μL, 1.15 mmol). The resulting yellow precipitate was separated by filtration, washed with ether (2 × 20 mL), and dried under vacuum. Yellow crystals of **4** (96 mg, 84%) were obtained by diffusion of ether vapor into an acetone solution.

(ii) A suspension of *exo*-**1** (46 mg, 0.094 mmol) in ether (20 mL) was treated with triflic acid (50 μL, 0.565 mmol). The resulting pale yellow precipitate was separated by filtration and washed with ether. Since the ^{1}H NMR spectrum showed the presence of some monoprotonated product,[11] the solid was dissolved in methanol (5 mL) and treated with another 50 μL portion of triflic acid to give a yellow solution. The solvent was removed under reduced pressure to give a brown oil, which solidified on addition of ether (20 mL). The product was recrystallized from acetone/ether to give **4** (64 mg, 86%). ^{1}H NMR (acetone-d_6, 300 MHz): δ 2.52 (q, J_{PH} = 0.7 Hz, C_6Me_6), 1.86 (vt, $^2J_{PH} + {}^4J_{PH}$ = 9.7 Hz, PMe_3). $^{31}P\{^1H\}$ NMR (acetone-d_6, 121.42 MHz): δ 5.83 (s). MS (electrospray (MeOH)): *m*/*z* 641, [M − CF_3SO_3]$^+$. Anal. Calcd for $C_{23}H_{45}F_6O_6RuP_3S_2$: C, 34.98; H, 5.74. Found: C, 34.60; H, 5.66.

(l) [Os(PMe$_3$)$_3$(η^6-C$_6$Me$_6$)](CF$_3$SO$_3$)$_2$ (5). (i) Treatment of a solution of *endo*-**2** (160 mg, 0.272 mmol) in ether (80 mL) with triflic acid (250 μL, 2.83 mmol) gave a brown solid, which was separated by filtration and washed with ether. The solid was redissolved in methanol (10 mL), and another 250 μL portion of triflic acid was added. Removal of the solvent under reduced pressure gave a brown oil which solidified on addition of ether (20 mL). Yellow crystals of **5** (190 mg, 80%) were obtained by vapor diffusion of ether into an acetone solution.

(ii) Treatment of a solution of *exo*-**2** (48 mg, 0.083 mmol) in ether (20 mL) with triflic acid (50 μL, 0.565 mmol) gave immediately an off-white precipitate, which was separated by filtration, washed with ether, and dissolved in methanol (5 mL). Addition of more triflic acid (50 μL, 0.565 mmol) gave a yellow solution. The solvent was removed under reduced pressure to give a brown oil, which solidified on addition of ether (20 mL). Recrystallization from acetone/ether gave off-white crystals of **5** (67 mg, 92%). ^{1}H NMR (acetone-d_6, 300 MHz): δ 2.53 (s, C_6Me_6), 1.93 (vt, $^2J_{PH} + {}^4J_{PH}$ = 9.7 Hz, PMe_3). $^{31}P\{^1H\}$ NMR (acetone-d_6, 121.42 MHz): δ −49.0 (s). MS (electrospray (MeOH)): *m*/*z* 731, [M − CF_3SO_3]$^+$. Anal. Calcd for $C_{23}H_{45}F_6O_6OsP_3S_2$: C, 31.43; H, 5.16; P, 10.57. Found: C, 31.56; H, 5.31; P, 10.46.

(m) [Os(PMe$_2$Ph)$_3$(η^6-C$_6$Me$_6$)](CF$_3$SO$_3$)$_2$ (6). (i) Addition of an excess of triflic acid (120 μL, 1.3 mmol) to a stirred solution of *endo*-**3** (53 mg, 0.069 mmol) in ether (20 mL) gave a deep yellow precipitate, which was separated by filtration, washed with ether (2 × 5 mL), and dried under vacuum. Yellow crystals of **6** (41 mg, 56%) were obtained by vapor diffusion of ether into an acetone solution.

(ii) A sample of *exo*-**3** (80 mg, 0.105 mmol) in ether (40 mL) was treated with two 100 μL portions of triflic acid, as described for *exo*-**1** and *exo*-**2**. After recrystallization from acetone/ether, **6** was obtained as an off-white solid (56 mg, 50%). ^{1}H NMR (CD_2Cl_2, 300 MHz): δ 7.7−7.2 (m, Ph), 2.13 (s, C_6Me_6), 2.06 (vt, $^2J_{PH} + {}^4J_{PH}$ = 8.9 Hz, PMe_2). $^{31}P\{^1H\}$ NMR (CD_2Cl_2, 121.42 MHz): δ −48.9 (s). MS (FAB): *m*/*z* 917, [M − CF_3SO_3]$^+$. Anal. Calcd for $C_{38}H_{52}F_6OsO_6P_3S_2$: C, 42.85; H, 4.83; S, 6.02. Found: C, 42.43; H, 4.51; S, 5.90.

(n) Os(PMe$_3$)$_4${κ^2-*o*-(CH$_2$)$_2$C$_6$Me$_4$} (8). A solution of *exo*-**2** (48 mg, 0.083 mmol) in toluene-d_8 (600 μL) was treated with PMe_3 (20 μL, 0.196 mmol). Removal of the volatile materials under reduced pressure gave **8** as a white crystalline solid (50 mg, 92%). X-ray-quality crystals were grown by slow evaporation of a solution in toluene-d_8. MS (EI): *m*/*z* (parent ion) calcd for $^{12}C_{24}{}^{1}H_{52}{}^{190}Os^{31}P_4$ 654.2604, found 654.2607; calcd for $^{12}C_{24}{}^{1}H_{52}{}^{192}Os^{31}P_4$ 656.2634, found 656.2624. Anal. Calcd for $C_{24}H_{52}OsP_4$: C, 44.03; H, 8.01; P, 18.92. Found: C, 44.29; H, 8.32; P, 18.67.

(o) Os(PMe$_2$Ph)$_4${κ^2-*o*-(CH$_2$)$_2$C$_6$Me$_4$} (9). A solution of *exo*-**3** (16 mg, 0.021 mmol) in toluene-d_8 (600 μL) was treated with PMe_2Ph (5 μL, 0.031 mmol). The solution was shown by ^{31}P NMR spectroscopy to contain an equilibrium mixture of *exo*-**3**, **9**, and PMe_2Ph. Complex **9** could not be isolated by column chromatography; it was therefore identified by comparison of its spectroscopic parameters with those of **8** (Table 2).

Deprotonation of [ML$_3$(η^6-C$_6$Me$_6$)]$^{2+}$. (a) A stirred suspension of complex **4** (M = Ru, L = PMe_3; 135 mg, 0.113 mmol) in THF (30 mL) was treated with an excess of KO-*t*-Bu (135 mg, 1.20 mmol) for 2 h. The solvent was removed under reduced pressure, and the resulting yellow residue was extracted with ether (3 × 10 mL). The extracts were filtered through Celite, and the ether was pumped off to give *endo*-**1** (50 mg, 91%).

(b) A stirred suspension of [Ru(PMe$_2$Ph)$_3$(η^6-C$_6$Me$_6$)](CF$_3$SO$_3$)$_2$ (400 mg, 0.410 mmol) in THF (50 mL) was treated with an excess of KO-*t*-Bu (460 mg, 4.10 mmol) for 30 min. Workup as described above gave Ru(PMe$_2$Ph)$_3${η^4-*exo*-(CH$_2$)$_2$C$_6$Me$_4$} (**7**; (212 mg, 77%), which was identified by its ^{1}H and $^{31}P\{^1H\}$ NMR spectra.[11]

(c) Treatment of complex **5** (M = Os, L = PMe_3; 160 mg, 0.182 mmol) in THF (30 mL) with an excess of KO-*t*-Bu (204 mg, 1.82 mmol) for 15 h as described above gave *endo*-**2** (99 mg, 94%). Similarly, complex **6** (M = Os, L = PMe_2Ph; 500 mg, 0.469 mmol) in THF (30 mL) with KO-*t*-Bu (526 mg, 4.69 mmol) for 16 h gave *endo*-**3** (242 mg, 67%).

Kinetics of *endo* to *exo* Isomerization. A sample of the *endo* isomer was dissolved under argon in toluene-d_8 in a 5 mm NMR tube. The initial concentrations (mmol per liter) were 34.0 (**1**), 20.2 (**2**), and 21.8 (**3**). The tube was placed in a Varian VXR-300S NMR spectrometer set at the desired temperature. The temperature was regulated by cooled gas flow and measured from the control panel after calibration with ethylene glycol and methanol NMR thermometers.[22] The rates of the isomerization were determined from the decrease of the integral of the well-separated higher field ^{1}H resonance at δ ca.4.5 of the pair associated with the *exo*-methylene protons of the *endo* isomer (see Table 1); data were collected at 15 min intervals. Line fitting and calculation of errors in

(22) Duerst, R.; Merbach, A. *Rev. Sci. Instrum.* **1965**, *36*, 1896.

Table 3. Crystal and Refinement Data for *endo*-1, *endo*-3, *exo*-3 and 8

	endo-**1**	*endo*-**3**	*exo*-**3**	**8**
		(a) Crystal Data		
chem formula	$C_{21}H_{43}P_3Ru$	$C_{36}H_{49}P_3Os$	$C_{36}H_{49}P_3Os$	$C_{24}H_{52}OsP_4$
fw	489.56	764.90	764.90	654.77
cryst syst	orthorhombic	monoclinic	triclinic	triclinic
unit cell dimens				
a (Å)	16.638(4)	15.956(2)	10.031(2)	9.290(3)
b (Å)	18.233(6)	13.159(4)	11.124(3)	12.936(3)
c (Å)	16.635(4)	16.262(3)	17.111(3)	13.085(2)
α (deg)			96.17(2)	86.48(2)
β (deg)		101.25(1)	90.88(2)	72.78(2)
γ (deg)			115.92(1)	78.02(2)
V (Å^3)	5046(2)	3355(1)	1703.2(7)	1469.3(6)
space group	*Pbca*	$P2_1/n$	$P\bar{1}$	$P\bar{1}$
D_c (g cm^{-3})	1.289	1.514	1.491	1.480
Z	8	4	2	2
F(000)	2064	1544	772	664
color, habit	yellow plate	yellow plate	yellow plate	colorless block
cryst dimens	0.88 × 0.18 × 0.32	0.32 × 0.28 × 0.06	0.20 × 0.15 × 0.03	0.53 × 0.32 × 0.24
μ (cm^{-1})	8.00 (Mo Kα)	87.06 (Cu Kα)	39.05 (Mo Kα)	45.67 (Mo Kα)
		(b) Data Collection and Processing		
diffractometer	Rigaku AFC 6S	Rigaku AFC 6R	Philips PW1100/20	Rigaku AFC 6S
X-radiation	Mo Kα	Cu Kα	Mo Kα	Mo Kα
scan mode	$\omega-2\theta$	$\omega-2\theta$	$\omega-2\theta$	$\omega-2\theta$
ω-scan width	1.20 + 0.34 tan θ	1.30 + 0.34 tan θ	1.00 + 0.34 tan θ	0.80 + 0.34 tan θ
2θ limits (deg)	50.1	120.2	48.0	50.1
min, max h,k,l	0−19, 0−21, 0−19	0−18, 0−15, −18 to +18	−11 to +11, −12 to +12, 0 to +19	0−11, −14 to +15, −14 to +15
no. of rflns				
total	4980	5449	5346	5557
unique (R_{int}/%)	4980	5241 (8.1)	5346	5206 (1.4)
obsd ($I > 3\sigma(I)$)	3238	3750	3786	4469
abs cor	azimuthal scans	azimuthal scans	DIFABS	azimuthal scans
min, max cor	0.7896, 1.0000	0.3398, 1.0000	0.7600, 1.0000	0.6300, 1.0000
		(c) Structure Analysis and Refinement		
structure solution	Patterson methods (DIRDIF92 PATTY)	Patterson methods (DIRDIF92 PATTY)	Patterson methods (DIRDIF92 PATTY)	Direct methods (SHELXS86)
refinement	full-matrix least squares	full-matrix least squares	full-matrix least squares	full-matrix least squares
no. of params	224	361	373	279
weighting scheme	$w = 4F_o^2/[\sigma^2(F_o^2) + (0.0200F_o^2)^2]$	$w = 4F_o^2/[\sigma^2(F_o^2) + (0.0040F_o^2)$	$w = 4F_o^2/[\sigma^2(F_o^2) + (0.0004F_o^2)^2]$	$w = 4F_o^2/[\sigma^2(F_o^2) + (0.0040F_o^2)^2]$
R(obsd data) (%)	3.2	3.7	3.7	2.5
R_w(obsd data) (%)	3.7	3.3	3.0	2.3

the activation parameters were performed with the IGOR PRO program.[23] The data are listed in the form k_{obs} (error) (10^6 s^{-1}) [T (K)]. *endo*-**1** → *exo*-**1**: no added PMe_3, 9.8 (0.3) [338.5], 15.6 (0.4) [343.0], 23.4 (0.6) [348.0], 37.0 (0.8) [353.0], 80.4 (4.6) [357.5], 100.7 (2.8) [361.5], 162.1 (3.9) [366.5], 209.2 (5.8) [368.5], 254.3 (8.1) [370.5], 324.3 (12.3) [373.0], 338.5 (11.3) [375.0], 393.3 (13.1) [377.0], 501.7 (18.9) [379.5]; with 20 equiv of added PMe_3, 13.1 (0.5) [348], 23.5 (0.5) [353.0], 27.6 (0.6) [357.5], 38.5 (1.0) [361.5], 71.8 (1.7) [366.5], 147.5 (3.6) [370.5], 263.4 (7.5) [375.0]. *endo*-**2** → *exo*-**2**: no added PMe_3, 6.5 (0.3) [357.5], 10.5 (0.3) [361.5], 18.9 (0.5) [366.5], 38.3 (0.8) [370.5], 66.3 (1.3) [375.0], 100.7 (2.3) [379.5]; with 20 equiv of added PMe_3, 7.5 (0.4) [353.0], 9.3 (0.4) [357.5], 12.8 (0.4) [361.5], 22.3 (0.5) [366.5], 30.6 (0.6) [370.5], 56.7 (1.0) [375.0]. *endo*-**3** → *exo*-**3**: no added PMe_2Ph, 3.0 (0.4) [338.5], 4.7 (0.5) [343.0], 12.6 (0.4) [348.0], 21.4 (2.2) [353.0], 42.5 (1.4) [357.5], 81.9 (3.5) [361.5], 179.6 (5.4) [366.5], 478.1 (19.0) [370.5], 994.5 (48.6) [375.0]; with 20 equiv of added PMe_2Ph, 3.3 (0.2) [343.0], 7.1 (0.4) [348.0], 13.0 (0.5) [353.0], 27.1 (0.9) [357.5], 46.1 (1.1) [361.5], 89.7 (2.4) [366.5], 136.3 (3.2) [370.5], 274.6 (8.2) [375.0].

The influence on the rate of isomerization k_{obs} of 0.5−20 mol of phosphine per mol of *endo* complex was studied. The data are listed in the form k_{obs} (error) (10^6 s^{-1}) [no. of equivalents of added phosphine]. *endo*-**1** → *exo*-**1** (T = 357.5 K): 80.4 (4.6) [0.0], 72.1 (2.9) [0.5], 46.6 (3.1) [1.0], 38.8 (2.7) [2.0], 23.3 (1.5) [4.0], 22.6 (1.1) [10.0], 27.5 (1.3) [20.0]. *endo*-**2** → *exo*-**2** (T = 379.5 K): 100.7 (2.3) [0.0], 109.8 (2.1) [1.0], 111.4 (2.3) [2.0], 114.5 (2.3) [4.0], 109.8 (2.1) [10.0], 117.3 (2.3) [20.0]. *endo*-**3** → *exo*-**3** (T = 357.5 K): 42.5 (1.4) [0.0], 41.5 (0.9) [0.5], 36.6 (0.9) [1.0], 34.8 (0.8) [2.0], 32.3 (0.8) [4.0], 31.8 (0.8) [10.0], 32.1 (0.8) [20.0].

The validity of the steady-state approximation (SSA) model used in the discussion of mechanism (see text) was checked by numerical simulations using two very different computational methods. The first was the deterministic approach,[24] in which the time dependence of the concentration of the various species is written as a set of coupled differential equations; these were integrated by means of the program REACT3.[25] The second was the stochastic method, in which changes in a reacting system are modeled by random selection among probability-weighted reaction steps; the program CKS was used for this purpose.[24,26−28]

Crystallography. The crystal and refinement data for $ML_3\{\eta^4\text{-}o\text{-}C_6Me_4(CH_2)_2\}$ (M = Ru, L = PMe_3, *exo*-**1**; M = Os, L = PMe_2Ph, *endo*- and *exo*-**3**) and $Os(PMe_3)_4\{\kappa^2\text{-}o\text{-}(CH_2)_2C_6Me_4\}$ (**8**) are summarized in Table 3. Crystals of *exo*-**1**, *exo*-**3**, and **8** were mounted under argon in Lindemann capillaries in silicone grease to prevent movement during data collection; a crystal of *endo*-**3** was mounted on a glass fiber with Araldite.

(23) IGOR PRO; Wave Metrics Inc., Lake Oswego, OR 97035, 1995.

(24) Steinfield, J. I.; Francisco, J. S.; Hase, W. L. *Chemical Kinetics and Dynamics*; Prentice Hall: Englewood Cliffs, NJ, 1989.

(25) Whitbeck, M. Numerical Modeling of Reaction Mechanisms. In *Tetrahedron Comput. Methodol.* **1992**, *3* (No. 6B), 497.

(26) Hinsberg, B.; Houle, F. A. CKS; IBM Research Division, Almaden Research Center, San Jose, CA 95120-6099.

(27) Bunker, D. L.; Garrett, B.; Kliendienst, T.; Long, G. S., III. *Combust. Flame* **1974**, *23*, 373.

(28) Gillespie, D. T. *J. Comput. Phys.* **1976**, *22*, 403.

The structures of *endo*- and *exo*-**3** and of *exo*-**1** were solved by Patterson methods (DIRDIF92, PATTY),[29] while the structure of **8** was solved by direct methods (SHELXS86).[30] All the structures were refined by full-matrix least-squares analysis. Hydrogen atoms were included at calculated positions (C−H = 0.95 Å) except for the methylene hydrogen atoms attached to carbon atoms C11 and C21 of *exo*-**3**, *exo*-**1**, and **8**, for which the coordinates were determined from an inner-data difference map and refined. Calculations were generally performed using the teXsan crystal structure analysis package.[31] The initial data reduction for *exo*-**3** was performed with the XTAL package.[32]

Computations. The electronic structure calculations are based on approximate density functional theory and were performed by use of the Amsterdam density functional (ADF) program developed by Baerends and co-workers.[33,34] The valence orbitals of the main-group elements were expanded in double-ζ Slater-type basis sets, augmented with a single p-type polarization function for hydrogen and a single d function for carbon and phosphorus. The orbitals of ruthenium were represented by a triple-ζ basis.[35] An auxiliary set of s, p, d, f, and g Slater functions was used to fit the molecular electron density.[36] Electrons in orbitals up to and including 1s (C), 2p (P), and 4p (Ru) were considered as cores and treated using the frozen-core approximation. Calculations were performed with the local exchange-correlation potential of Vosko, Wilk, and Nusair,[37] along with the gradient corrections of Becke[38] and Perdew.[39] Quasi-relativistic corrections were made for both ruthenium and osmium. Geometries were optimized in C_{2v} (κ^2-M(PH$_3$)$_4$(C$_8$H$_8$)), C_s (*endo*- and *exo*-M(PH$_3$)$_3$(C$_8$H$_8$)), and C_{3v} (PH$_3$) symmetry using the gradient algorithm of Versluis and Ziegler.[40]

Results

In contrast with the behavior of the Ru−PMe$_2$Ph system (eq 1),[11] treatment of [Ru(O$_2$CCF$_3$)(PMe$_3$)$_2$(η^6-C$_6$Me$_6$)]PF$_6$ with KO-*t*-Bu in the presence of trimethylphosphine gives exclusively the *endo*-(tetramethyl-*o*-xylylene)ruthenium(0) complex Ru(PMe$_3$)$_3${η^4-*endo*-*o*-C$_6$Me$_4$(CH$_2$)$_2$} (*endo*-**1**) in 88% yield as a yellow, air-sensitive, crystalline solid. Similarly, reaction of the osmium(II) salts [Os(O$_2$CCF$_3$)L$_2$(η^6-C$_6$Me$_6$)]PF$_6$ (L = PMe$_3$, PMe$_2$Ph) with KO-*t*-Bu and L gives the corresponding *endo*-(tetramethyl-*o*-xylylene)osmium(0) complexes OsL$_3${η^4-*endo*-*o*-C$_6$Me$_4$(CH$_2$)$_2$} (L = PMe$_3$ (*endo*-**2**), PMe$_2$Ph (*endo*-**3**)) (eq 3). The new compounds have been characterized by elemental analysis, mass spectrometry, infrared and NMR (^{1}H, ^{13}C, and ^{31}P) spectroscopy (Table 1) and, in the case of *endo*- and *exo*-**3**, by single-crystal X-ray structure analysis (see below). As in M(PMe$_2$Ph)$_3${η^4-*endo*-*o*-C$_6$H$_4$(CH$_2$)$_2$} (M = Ru, Os),[12] the trigonal ML$_3$ fragment is bound to the *endo*-diene unit, a pair of tertiary phosphine ligands being related by a mirror plane that bisects the tetramethyl-*o*-xylylene, and a unique tertiary phosphine lying in the mirror plane below the coordinated diene.

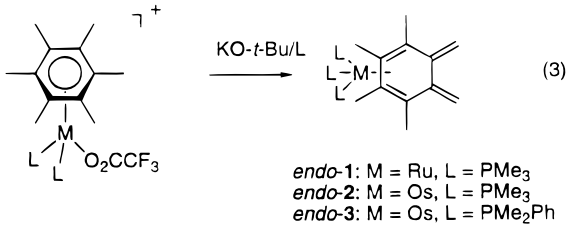

(3)

endo-**1**: M = Ru, L = PMe$_3$
endo-**2**: M = Os, L = PMe$_3$
endo-**3**: M = Os, L = PMe$_2$Ph

The spectroscopic properties of *endo*-**1**−**3** are generally similar to those of M(PMe$_2$Ph)$_3${η^4-*endo*-*o*-C$_6$H$_4$(CH$_2$)$_2$} (M = Ru, Os).[12] The IR spectra contain a weak band in the 1500−1600 cm^{-1} region assignable to ν(C=C) of the uncoordinated *exo*-diene. The ^{1}H NMR spectra show a characteristic pair of multiplets at δ ca. 4.5 and 5.3 due to the *exo*-methylene protons, and a singlet at δ ca. 90 in the ^{13}C NMR spectra is assigned to the *exo*-methylene carbon atoms. The inner carbon atoms of the *exo*-diene give rise to a doublet at δ ca. 155, being coupled to only one of the three phosphorus atoms ($^2J_{PC}$ ca. 4 Hz). The inner carbon atoms C^{4,5} of the coordinated *endo*-diene appear at δ ca. 80; for *endo*-**1** and *endo*-**3** this resonance is a doublet owing to coupling with the unique phosphorus atom (P^1), whereas for *endo*-**2** the resonance is a doublet of triplets because of additional weaker coupling with the other two, equivalent phosphorus atoms (P^2, P^3). For similar reasons, the outer carbon atoms C^{3,6} of the *endo*-diene also appear as a doublet of triplets, at δ ca. 25 for *endo*-**1** and at 50 for *endo*-**2** and *endo*-**3**; surprisingly, the trend of chemical shifts is opposite to that shown for the outer diene carbon atoms in M(CO)$_3$(η^4-1,3-diene) (M = Fe, Ru, Os), which become progressively more shielded with increasing atomic number of the metal.[41] The ring methyl protons (Me−C^{3,6} and Me−C^{4,5}) appear as a pair of well-resolved multiplets owing to ^{31}P coupling. The ^{31}P{^{1}H} NMR spectra of *endo*-**3** show a well-resolved doublet and triplet ($^2J_{PP}$ ca. 5−11 Hz) in the expected 2:1 intensity ratio; in contrast to M(PMe$_2$Ph)$_3${η^4-*endo*-*o*-C$_6$H$_4$(CH$_2$)$_2$} (M = Ru, Os), rotation of the tertiary phosphine ligands relative to the coordinated diene is slow on the NMR time scale at room temperature.

Treatment of complexes *endo*-**1**−**3** with an excess of triflic acid (CF$_3$SO$_3$H, TfOH) in ether precipitates the triflate salts of the hexamethylbenzene−metal(II) cations, [ML$_3$(η^6-C$_6$Me$_6$)](OTf)$_2$ (L = PMe$_3$, M = Ru (**4**), Os (**5**); L = PMe$_2$Ph, M = Os (**6**)) (eq 4). These have been characterized by elemental analysis and by their spectroscopic properties, which are unexceptional (see Experimental Section). Reaction of complexes **4**−**6** with KO-*t*-Bu re-forms the tetramethyl-*o*-xylylene complexes *endo*-**1**−**3**, just as the parent *endo*-*o*-xylylene complexes M(PMe$_2$Ph)$_3${η^4-*endo*-*o*-C$_6$H$_4$(CH$_2$)$_2$} are generated from the corresponding (*o*-xylene)metal dications [M(PMe$_2$Ph)$_3$(η^6-C$_6$H$_4$Me$_2$)]$^{2+}$.[12] In contrast, treatment of a

(29) Beurskens, P. T.; Admiraal, G.; Beurskens, G.; Bosman, W. P.; Garcia-Granda, S.; Gould, R. O.; Smits, J. M. M.; Symkalla, C. The DIRDIF Program System; Technical Report of the Crystallography Laboratory; University of Nijmegen, Nijmegen, The Netherlands, 1992.
(30) Sheldrick, G. M. SHELX-86. In *Crystallographic Computing 3*; Sheldrick, G. M., Krüger, C., Goddard, R., Eds.; Oxford University Press: Oxford, England, 1985; pp 175−189.
(31) TEXSAN: Single-Crystal Structure Analysis Software, Version 1.6c; Molecular Structure Corp., The Woodlands, TX 77381, 1993.
(32) Hall, S. R.; Flack, H. D.; Stewart, J. M. *XTAL3.2 Reference Manual*; Universities of Western Australia, Geneva and Maryland; Lamb: Perth, Australia, 1992.
(33) Baerends, E. J.; Ellis, D. E.; Ros, P. *Chem. Phys.* **1973**, *2*, 41.
(34) te Velde, G. B.; Baerends, E. J. *J. Comput. Phys.* **1992**, *99*, 84.
(35) Vernooijs, P.; Snijders, G. J.; Baerends, E. J. *Slater Type Basis Functions for the Whole Periodic System*; Free University of Amsterdam: Amsterdam, The Netherlands, 1981.
(36) Krijn, J.; Baerends, E. J. *Fit Functions in the HFS Method*; Free University of Amsterdam: Amsterdam, The Netherlands, 1984.
(37) Vosko, S. H.; Wilk, L.; Nusair, M. *Can. J. Phys.* **1980**, *58*, 1200.
(38) Becke, A. D. *Phys. Rev. A* **1988**, *38*, 3098.
(39) Perdew, J. P. *Phys. Rev. B* **1986**, *33*, 8822.
(40) Versluis, L.; Ziegler, T. *J. Chem. Phys.* **1988**, *88*, 322.
(41) Zobl-Ruh, S.; von Philipsborn, W. *Helv. Chim. Acta* **1980**, *63*, 773.

Scheme 1

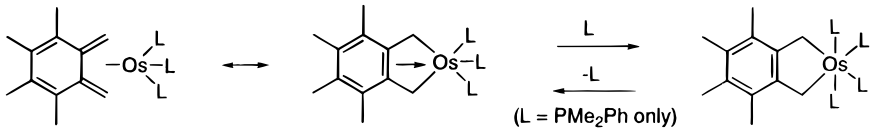

endo-**2**
endo-**3**

8: L = PMe_3
9: L = PMe_2Ph

suspension of $[Ru(PMe_2Ph)_3(\eta^6\text{-}C_6Me_6)](OTf)_2$[11] in THF with KO-*t*-Bu forms exclusively the *exo*-tetramethyl-*o*-xylylene complex $M(PMe_2Ph)_3\{\eta^4\text{-}exo\text{-}o\text{-}(CH_2)_2C_6Me_4\}$ (**7**) (eq 5).

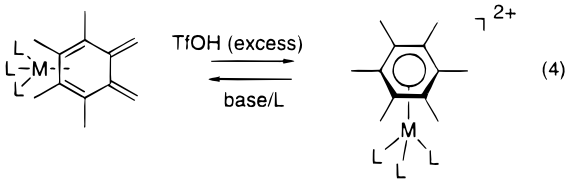

(4)

4: M = Ru, L = PMe_3
5: M = Os, L = PMe_3
6: M = Os, L = PMe_2Ph

This remarkable difference of regioselectivity in deprotonation for the Ru−PMe_2Ph and Os−PMe_2Ph systems suggested that *endo* to *exo* isomerization might be observable in tetramethyl-*o*-xylylene complexes. Indeed, heating in toluene above 65 °C causes quantitative isomerization of the *endo* complexes **1**−**3** to the corresponding *exo* complexes $ML_3\{\eta^4\text{-}exo\text{-}o\text{-}(CH_2)_2C_6Me_4\}$ (L = PMe_3, M = Ru (*exo*-**1**), Os (*exo*-**2**); L = PMe_2Ph, M = Os (*exo*-**3**)) (eq 6), whose NMR properties (Table 1) are

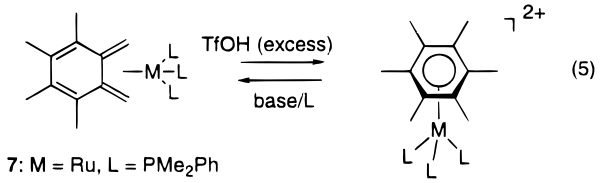

(5)

7: M = Ru, L = PMe_2Ph

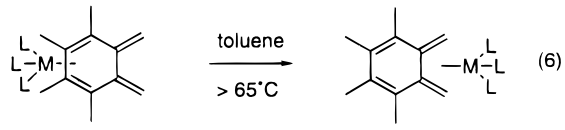

(6)

endo-**1**
endo-**2**
endo-**3**

exo-**1**: M = Ru, L = PMe_3
exo-**2**: M = Os, L = PMe_3
exo-**3**: M = Os, L = PMe_2Ph

similar to those of previously described analogues, such as complex **7**.[11] In particular, the ^1H NMR spectra show a characteristic pair of multiplets at δ 0 to −0.4 and 2.0−2.5 due to *anti* and *syn* protons of the coordinated *exo*-1,3-diene. A multiplet at δ 22−27 in the ^{13}C NMR spectrum is assigned to the *exo*-methylene carbon atoms, shifted by ca. 70 ppm to lower frequency of the corresponding resonance in *endo*-**1**−**3**. The inner diene carbon atoms $C^{1,2}$ resonate at δ ca. 100, ca. 50 ppm to low frequency of their chemical shift in **1**−**3**. The $^{31}P\{^1H\}$ NMR spectra of the *exo* complexes, like those of their *endo* isomers, show a well-resolved doublet and triplet ($^2J_{PP}$ = ca. 6−12 Hz) in an intensity ratio of 2:1. The structures of *exo*-**1** and *exo* **3** have been confirmed by single-crystal X-ray diffraction analysis (see below). Treatment of the *exo*-isomers with an excess of triflic acid regenerates the triflate salts of the (hexamethylbenzene)metal dications **4**−**6**, which were isolated in good yield (eq 5).

We reported previously[12] that the unsubstituted complex $Ru(PMe_2Ph)_3\{\eta^4\text{-}endo\text{-}o\text{-}C_6H_4(CH_2)_2\}$ does not isomerize to the *exo* compound in toluene at or above 60 °C, even though the *exo* isomer is predicted to be the more stable.[16] We now find that this isomerization proceeds quantitatively in the molten state (ca. 300 °C); the osmium compound decomposes under these conditions.

While studying the effect of added tertiary phosphine on the kinetics of the thermal *endo* to *exo* isomerization of the osmium complexes **2** and **3** (see below), we realized that the products under these conditions are the κ^2-3,4,5,6-tetramethyl-*o*-xylylene tetrakis(tertiary phosphine) complexes $OsL_4\{\kappa^2\text{-}o\text{-}(CH_2)_2C_6Me_4\}$ (L = PMe_3 (**8**), PMe_2Ph (**9**)) rather than the tris(tertiary phosphine) complexes *exo*-**2** and *exo*-**3**. The added ligand can be considered to displace the coordinated formal double bond of the aromatic ring of the *o*-xylylene (Scheme 1). Complex **8** can be isolated in 92% yield as a colorless, crystalline solid from the reaction of PMe_3 with *exo*-**2** at room temperature. It has been characterized by elemental analysis, mass spectrometry, NMR (^1H, ^{13}C, and ^{31}P) spectroscopy, and single-crystal X-ray diffraction (see below). Complex **9** cannot be isolated and has been characterized only on the basis of its NMR spectroscopic data. It is in rapid equilibrium with *exo*-**3** and free PMe_2Ph, the equilibrium constant for the reaction

$$Os(PMe_2Ph)_3\{\eta^4\text{-}exo\text{-}o\text{-}(CH_2)_2C_6Me_4\} + PMe_2Ph \rightleftarrows Os(PMe_2Ph)_4\{\kappa^2\text{-}o\text{-}(CH_2)_2C_6Me_4\}$$

measured by ^{31}P NMR spectroscopy being 1.10 ± 0.02 at 25 °C. The highest mass peak in the EI mass spectrum of toluene solutions of **9** is that due to **3**, showing that **9** is stable only in the presence of free PMe_2Ph. In contrast, there is no evidence for the presence of *exo*-**2** and PMe_3 in solutions of **8** and there is no observable reaction between the ruthenium complex *exo*-**1** and PMe_3.

The ^1H NMR spectra of **8** and **9** each show a resonance at δ ca. 2.3, which appears as a triplet of triplets owing to coupling with two pairs of inequivalent ^{31}P nuclei, and is assigned to the equivalent methylene protons. The $^{31}P\{^1H\}$ NMR spectra consist of a pair of 1:2:1 triplets of equal intensity ($^2J_{PP}$ = 16.5 Hz for **8** and 13.1 Hz for **9**) arising from two pairs of tertiary phosphines: one mutually trans, the other cis. In the ^{13}C NMR spectra the methylene carbon atoms give resonances at δ ca. 9, which for **9** is a triplet with separations of 16.5 Hz and for **8** is a double triplet of doublets with separations of 45.5, 9.1, and 4.8 Hz. The

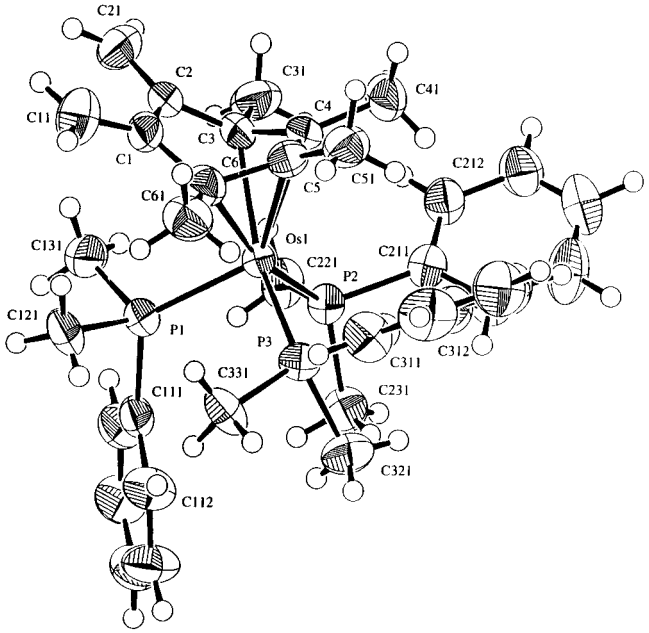

Figure 2. Molecular structure of $Os(PMe_2Ph)_3\{\eta^4\text{-}endo\text{-}o\text{-}C_6Me_4(CH_2)_2\}$ (*endo*-**3**) with 50% ellipsoids.

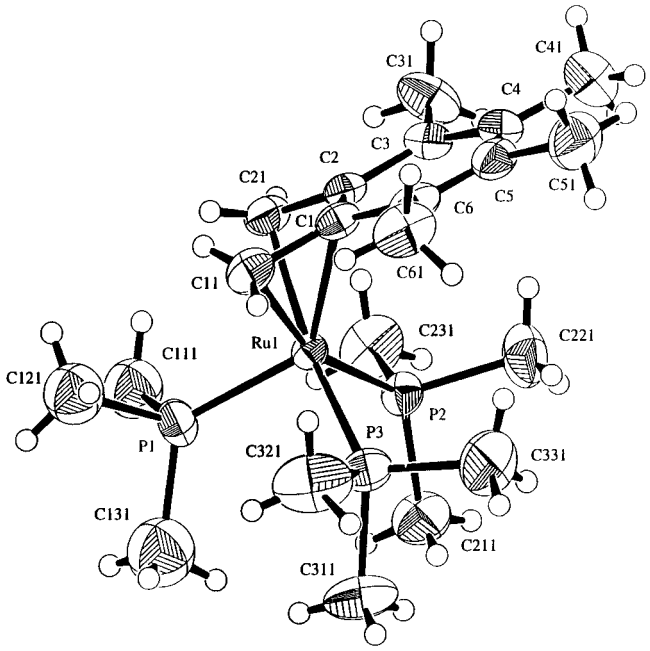

Figure 3. Molecular structure of $Ru(PMe_3)_3\{\eta^4\text{-}exo\text{-}o\text{-}(CH_2)_2C_6Me_4\}$ (*exo*-**1**) with 50% ellipsoids.

signals due to carbon atoms C^1 and C^2 to which the methylene groups are attached occur as doublets of triplets at δ ca. 153 with separations of ca. 10 and 5 Hz, while the signals due to the remaining ring carbon atoms $C^{3,6}$ and $C^{4,5}$ appear in the normal aromatic region at δ ca. 130. Relative to the corresponding chemical shifts in *exo*-**2** and *exo*-**3**, the ca. 14 ppm shift to low frequency of the methylene carbon atoms in **8** and **9**, and the ca. 55 ppm shift to high frequency of the now uncoordinated carbon atoms C^1 and C^2, are diagnostic of the change from η^4-*exo* to κ^2 binding of the tetramethyl-*o*-xylylene unit.

Crystal and Molecular Structures. The molecular structures of $Os(PMe_2Ph)_3\{\eta^4\text{-}endo\text{-}o\text{-}C_6Me_4(CH_2)_2\}$ (*endo*-**3**), $Ru(PMe_3)_3\{\eta^4\text{-}exo\text{-}o\text{-}(CH_2)_2C_6Me_4\}$ (*exo*-**1**), $Os(PMe_2Ph)_3\{\eta^4\text{-}exo\text{-}o\text{-}(CH_2)_2C_6Me_4\}$ (*exo*-**3**), and $Os(PMe_3)_4\{\kappa^2\text{-}o\text{-}(CH_2)_2C_6Me_4\}$ (**8**) are shown in Figures 2−5, with the atom numbering; selected bond distances and interatomic angles are given in Tables 4−7. The geometry of *endo*-**3** is very similar to that of the unsubstituted compound $Os(PMe_2Ph)_3\{\eta^4\text{-}endo\text{-}o\text{-}C_6H_4(CH_2)_2\}$.[12] The $Os(PMe_2Ph)_3$ moiety is bound to the endocyclic diene unit, the metal atom being slightly closer to the inner than to the outer carbon atoms (Os−C(4),C(5) = 2.230 Å (average), Os−C(3),C(6) = 2.279 Å (average)). These distances are, respectively, ca. 0.06 and 0.03 Å greater than the corresponding separations in the unsubstituted compound.[12] The *o*-xylylene ring in *endo*-**3** has the characteristic folded conformation, the dihedral angle between the C(3) to C(6) and C(6)−C(1)−C(2)−C(3) planes being 42.9° (cf. 37.0 and 39.5° in the unsubstituted Ru and Os compounds[12] and 33.8° in $Ru(\eta^6\text{-}C_6Me_6)\{\eta^4\text{-}endo\text{-}o\text{-}C_6Me_4(CH_2)_2\}$.[4]

In the *exo* isomers of **1** and **3**, the ML_3 fragments are bound to the exocyclic diene unit, the geometries being similar to that of the unsubstituted compound $Ru(PMe_2Ph)_3\{\eta^4\text{-}exo\text{-}o\text{-}(CH_2)_2C_6H_4\}$.[13] In contrast to *endo*-**3**, the metal atoms in *exo*-**1** and *exo*-**3** are considerably closer to the outer than to the inner diene carbon atoms (Ru−C(11),C(21) = 2.173 Å (average), Ru−C(1),C(2) = 2.291

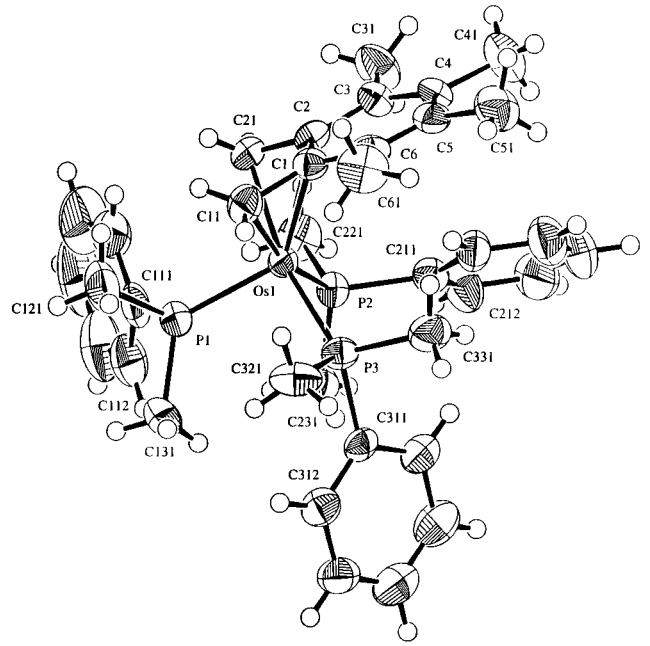

Figure 4. Molecular structure of $Os(PMe_2Ph)_3\{\eta^4\text{-}exo\text{-}o\text{-}(CH_2)_2C_6Me_4\}$ (*exo*-**3**) with 50% ellipsoids.

Å (average) in *exo*-**1**; Os−C(11),C(21) = 2.172 Å (average), Os−C(1),C(2) = 2.324 Å (average) in *exo*-**3**). As discussed previously,[16] this reversal of the normal trend for (1−4-η)-diene complexes can be ascribed to the tendency toward aromatization of the six-membered ring in the *exo*-η^4 complexes. The Ru−C(diene) distances in *exo*-**1** are close to those observed in $Ru(PMe_2Ph)_3\{\eta^4\text{-}exo\text{-}o\text{-}(CH_2)_2C_6H_4\}$;[13] i.e., they are unaffected by the methyl substitution in the six-membered ring. As in other *exo*-*o*-xylylene complexes, such as $Co(\eta^5\text{-}C_5H_5)\{\eta^4\text{-}o\text{-}(CH_2)_2C_6H_4\}$[7] and $Fe(CO)_3\{\eta^4\text{-}o\text{-}(CH_2)_2C_6H_2Me_2\text{-}4,5\}$,[42] but in contrast with *endo*-**3**, the *o*-xylylene ring

(42) Girard, L.; Decken, A.; Blecking, A.; McGlinchey, M. J. *J. Am. Chem. Soc.* **1994**, *116*, 6427.

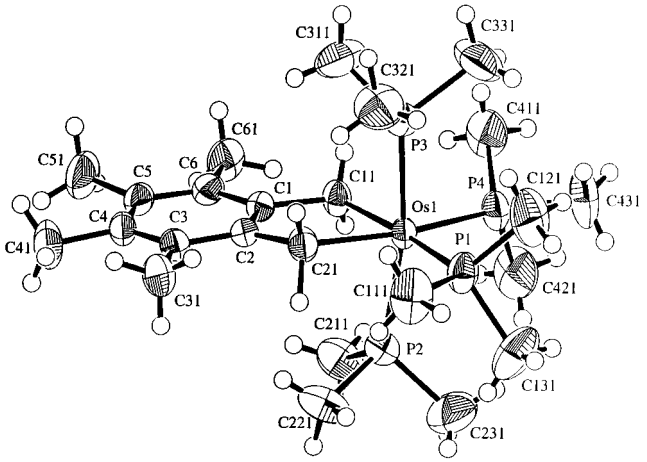

Figure 5. Molecular structure of $Os(PMe_3)_4\{\kappa^2\text{-}o\text{-}(CH_2)_2C_6Me_4\}$ (**8**) with 50% ellipsoids.

Table 4. Selected Bond Lengths (Å) for $Os(PMe_2Ph)_3\{\eta^4\text{-}endo\text{-}o\text{-}C_6Me_4(CH_2)_2\}$ (*endo*-3)

Os(1)−P(1)	2.296(2)	Os(1)−P(2)	2.338(2)
Os(1)−P(3)	2.328(2)	Os(1)−C(3)	2.281(8)
Os(1)−C(4)	2.226(8)	Os(1)−C(5)	2.234(8)
Os(1)−C(6)	2.276(8)		
P(1)−C(111)	1.868(8)	P(1)−C(121)	1.806(10)
P(1)−C(131)	1.845(9)	P(2)−C(211)	1.843(8)
P(2)−C(221)	1.843(8)	P(2)−C(231)	1.840(8)
P(3)−C(311)	1.884(9)	P(3)−C(321)	1.824(9)
P(3)−C(331)	1.855(8)		
C(1)−C(11)	1.32(1)	C(1)−C(2)	1.47(1)
C(2)−C(21)	1.34(1)	C(2)−C(3)	1.45(1)
C(3)−C(31)	1.52(1)	C(3)−C(4)	1.45(1)
C(4)−C(41)	1.53(1)	C(4)−C(5)	1.38(1)
C(5)−C(51)	1.53(1)	C(5)−C(6)	1.47(1)
C(6)−C(1)	1.47(1)	C(6)−C(61)	1.50(1)

Table 5. Selected Bond Lengths (Å) for $Ru(PMe_3)_3\{\eta^4\text{-}exo\text{-}(CH_2)_2C_6Me_4\}$ (*exo*-1)

Ru(1)−P(1)	2.238(1)	Ru(1)−P(2)	2.306(1)
Ru(1)−P(3)	2.311(1)	Ru(1)−C(1)	2.284(4)
Ru(1)−C(2)	2.297(4)	Ru(1)−C(11)	2.170(4)
Ru(1)−C(21)	2.175(4)		
P(1)−C(111)	1.869(1)	P(1)−C(111′)	1.81(1)
P(1)−C(121)	1.82(1)	P(1)−C(121′)	1.84(1)
P(1)−C(131)	1.82(2)	P(1)−C(131′)	1.85(1)
P(2)−C(211)	1.824(5)	P(2)−C(221)	1.829(5)
P(2)−C(311)	1.837(5)	P(3)−C(311)	1.837(5)
P(3)−C(321)	1.841(5)	P(3)−C(331)	1.812(6)
C(1)−C(11)	1.461(6)	C(1)−C(2)	1.428(5)
C(2)−C(21)	1.451(5)	C(2)−C(3)	1.440(6)
C(3)−C(31)	1.498(6)	C(3)−C(4)	1.362(6)
C(4)−C(41)	1.539(6)	C(4)−C(5)	1.414(6)
C(5)−C(51)	1.516(6)	C(5)−C(6)	1.376(6)
C(6)−C(1)	1.433(6)	C(6)−C(61)	1.519(6)

in *exo*-**1** and *exo*-**3** is almost flat, the dihedral angle between the C(3) to C(6) and C(6)−C(1)−C(2)−C(3) planes being 1.9° (*exo*-**1**) and 4.3° (*exo*-**3**). In all three tetramethyl-*o*-xylylene complexes, the C−C bond lengths within the uncoordinated diene fragment show the expected short−long−short alternation, whereas those in the coordinated diene unit are almost equal.

In agreement with the spectroscopic studies, the X-ray structure analysis of **8** shows that the tetramethyl-*o*-xylylene is bound to the $Os(PMe_3)_4$ unit via the two exocyclic methylene groups, so that the ligand behaves as a two-electron σ-donor. The distorted-octahedral geometry about the metal atom is similar to that observed in $Mn(dmpe)_2\{\kappa^2\text{-}o\text{-}(CH_2)_2C_6H_4\}$ (dmpe = 1,2-bis(dimethylphosphino)ethane, $Me_2PCH_2CH_2PMe_2$)[43] and

Table 6. Selected Bond Lengths (Å) for $Os(PMe_2Ph)_3\{\eta^4\text{-}exo\text{-}(CH_2)_2C_6Me_4\}$ (*exo*-3)

Os(1)−P(1)	2.257(2)	Os(1)−P(2)	2.308(2)
Os(1)−P(3)	2.316(2)	Os(1)−C(1)	2.337(7)
Os(1)−C(2)	2.310(7)	Os(1)−C(11)	2.187(9)
Os(1)−C(21)	2.157(8)		
P(1)−C(111)	1.839(9)	P(1)−C(121)	1.821(9)
P(1)−C(131)	1.826(8)	P(2)−C(211)	1.857(8)
P(2)−C(221)	1.824(8)	P(2)−C(231)	1.840(8)
P(3)−C(311)	1.843(8)	P(3)−C(321)	1.839(8)
P(3)−C(331)	1.843(8)		
C(1)−C(11)	1.45(1)	C(1)−C(2)	1.444(9)
C(2)−C(21)	1.44(1)	C(2)−C(3)	1.429(9)
C(3)−C(31)	1.51(1)	C(3)−C(4)	1.384(10)
C(4)−C(41)	1.51(1)	C(4)−C(5)	1.43(1)
C(5)−C(51)	1.50(1)	C(5)−C(6)	1.367(10)
C(6)−C(1)	1.420(10)	C(6)−C(61)	1.51(1)

Table 7. Selected Bond Lengths for $Os(PMe_3)_4\{\kappa^2\text{-}o\text{-}(CH_2)_2C_6Me_4\}$ (8)

Os(1)−P(1)	2.308(2)	Os(1)−P(2)	2.349(2)
Os(1)−P(3)	2.343(2)	Os(1)−P(4)	2.316(1)
Os(1)−C(11)	2.170(5)	Os(1)−C(21)	2.185(5)
P(1)−C(111)	1.835(6)	P(1)−C(121)	1.854(7)
P(1)−C(131)	1.842(6)	P(2)−C(211)	1.826(6)
P(2)−C(221)	1.835(6)	P(2)−C(231)	1.846(6)
P(3)−C(311)	1.830(6)	P(3)−C(321)	1.852(6)
P(3)−C(331)	1.853(6)	P(4)−C(411)	1.847(6)
P(3)−C(421)	1.857(6)	P(4)−C(431)	1.834(6)
C(1)−C(11)	1.527(6)	C(1)−C(2)	1.398(6)
C(2)−C(21)	1.498(7)	C(2)−C(3)	1.413(6)
C(3)−C(31)	1.534(7)	C(3)−C(4)	1.384(7)
C(4)−C(41)	1.524(7)	C(4)−C(5)	1.401(7)
C(5)−C(51)	1.524(7)	C(5)−C(6)	1.404(6)
C(6)−C(1)	1.394(6)	C(6)−C(61)	1.507(7)

in $Os(PMe_3)_4\{\kappa^2\text{-}o\text{-}(CH_2)_2SiMe_2\}$.[44] The Os−C distances in **8** differ slightly (2.170(5), 2.185(5) Å), possibly as a consequence of solid-state effects; they are somewhat less than those in $Os(PMe_3)_4\{\kappa^2\text{-}o\text{-}(CH_2)_2SiMe_2\}$ (2.24(1) Å) but are similar to the Os−CH_3 distances in $OsI(Me)(CO)_2(PMe_3)_2$ (2.174(15) Å) and $[OsMe(CO)_2(NCMe)(PMe_3)_2]BPh_4$ (2.198(17) Å).[45] As in $Os(PMe_3)_4\{\kappa^2\text{-}o\text{-}(CH_2)_2SiMe_2\}$, the Os−P bond lengths for phosphorus trans to phosphorus (2.349(2), 2.343(2) Å) in **8** are greater than those for phosphorus trans to carbon (2.308(2), 2.316(1) Å). The bond distances within the six-membered ring (C(1)−C(6)) of **8** fall in a closer range (1.384−1.413 Å) than those in *exo*-**3** (1.367−1.444 Å), consistent with the greater aromatic character of the ring in the former compound. The *o*-xylylene ring in **8** is almost flat, the dihedral angle between the planes C(11)−C(1)−C(2)−C(21) and Os(1)−C(11)−C(21) being only 6.6° (cf. 89.4° in *exo*-**3**). The magnitude of this fold angle in the compounds formulated as κ^2-*o*-xylylene complexes is remarkably variable, e.g., 3.9° in $Mn(dmpe)_2\{\kappa^2\text{-}o\text{-}(CH_2)_2C_6H_4\}$,[43] 41−53° in $M(\eta^5\text{-}C_5H_5)_2\{o\text{-}(CH_2)_2C_6H_4\}$ (M = Ti, Zr, Hf),[9] 44° in $Nb(\eta^5\text{-}C_5H_4SiMe_3)_2\{o\text{-}(CH_2)_2C_6H_4\}$,[9] 66 and 42° in $Mg(thf)_4[OW\{o\text{-}(CH_2)_2C_6H_4\}_2]$,[10] and 83° in $W\{o\text{-}(CH_2)_2C_6H_4\}_3$.[10] It has been suggested[10] that the larger values reflect a π-interaction of the aromatic ring with the metal center.

Computational Results. In an effort to understand better the different behavior of the *o*-xylylene complexes of ruthenium(0) and osmium(0) with ligands, we carried

(43) Howard, C. G.; Girolami, G. S.; Wilkinson, G.; Thornton-Pett, M.; Hursthouse, M. B. *J. Chem. Soc., Dalton Trans.* **1983**, 2631.
(44) Behling, T.; Girolami, G. S.; Wilkinson, G.; Somerville, R. G.; Hursthouse, M. B. *J. Chem. Soc., Dalton Trans.* **1984**, 877.
(45) Bellachioma, G.; Cardaci, G.; Macchioni, A.; Zanazzi, P. *Inorg. Chem.* **1993**, *32*, 547.

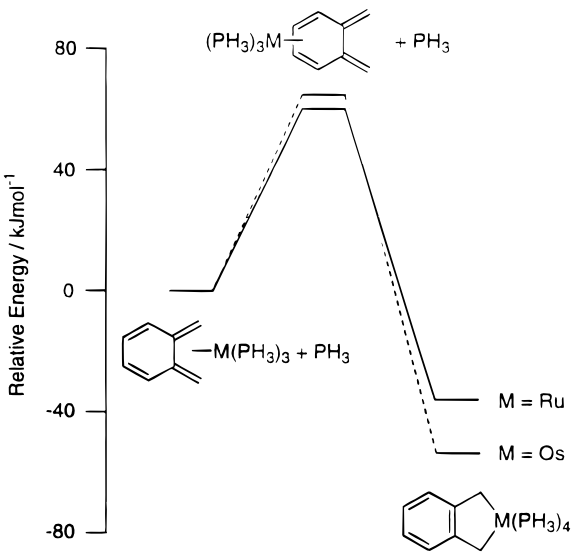

Figure 6. Energy level diagram showing the calculated relative energies of η^4-*endo*-, η^4-*exo*-, κ^2-*o*-xylylene complexes of ruthenium and osmium.

Table 8. Calculated Total Energies (eV) of *endo*- and *exo*-$ML_3\{\eta^4$-*o*-$C_6H_4(CH_2)_2\}$ and of $ML_4\{\kappa^2$-*o*-$(CH_2)_2C_6H_4\}$ (M = Ru, Os; L = PH_3)

molecular fragment	energy
PH_3	−15.19
exo- $Ru(PH_3)_3$(*o*- xylylene)	−152.89
endo- $Ru(PH_3)_3$(*o*- xylylene)	−152.25
$Ru(PH_3)_4$(*o*- xylylene)	−168.42
exo- $Os(PH_3)_3$(*o*- xylylene)	−153.49
endo- $Os(PH_3)_3$(*o*- xylylene)	−152.81
$Os(PH_3)_4$(*o*- xylylene)	−169.24

out density functional calculations on the model systems $M(PH_3)_3\{\eta^4$-*endo*-*o*-$C_6H_4(CH_2)_2\} + PH_3$, $M(PH_3)_3\{\eta^4$-*exo*-*o*-$(CH_2)_2C_6H_4\} + PH_3$, and $M(PH_3)_4\{\kappa^2$-*o*-$(CH_2)_2C_6H_4\}$ (M = Ru, Os). The energies are listed in Table 8 and represented graphically in Figure 6, where the energies are plotted relative to those of $M(PH_3)_3\{\eta^4$-*exo*-*o*-$(CH_2)_2C_6H_4\}$. For both ruthenium and osmium the *exo* isomer is more stable than the *endo* isomer by ca. 60 kJ mol^{-1}. As shown earlier,[16] this can be attributed largely to the tendency toward aromatization of the six-membered ring; hence, the identity of the metal atom plays only a small role in determining the relative stability of the *endo* and *exo* isomers. For both metals, the κ^2 complex is found to be more stable than (η^4-*exo*-complex + PH_3), by ca. 36 kJ mol^{-1} for Ru and ca. 53 kJ mol^{-1} for Os. The relationship of these predictions to the experimental results is discussed below.

Kinetics of Isomerization. The *endo* to *exo* isomerizations of complexes **1**−**3** in toluene-d_8 exhibit good first-order kinetics in the temperature range 65−106 °C, as established by ^{1}H NMR spectroscopy. Figure 7 shows typical first-order rate plots at eight temperatures for the disappearance of *endo*-**3**, Figure 8 shows the derived Eyring plot, and Table 9 summarizes the activation parameters for the *endo*- to *exo*-isomerizations of **1**−**3**.

As shown in Figure 9, the rate of isomerization of the ruthenium−PMe_3 complex, *endo*-**1**, is reduced exponentially by addition of small amounts of PMe_3; the rate constant is approximately halved in the presence of 2 mmol of PMe_3 per mmol of *endo*-**1**, but it rapidly reaches

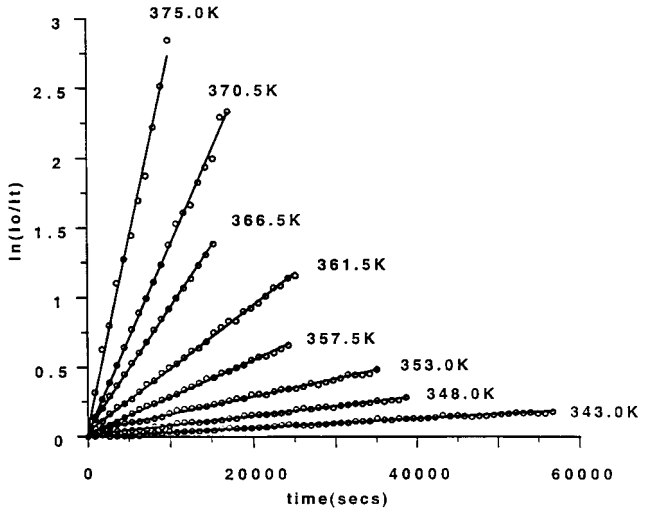

Figure 7. First-order rate plots from NMR spectroscopy for the *endo* to *exo* isomerization of $Os(PMe_2Ph)_3\{\eta^4$-*o*-$C_6Me_4(CH_2)_2\}$ (**3**).

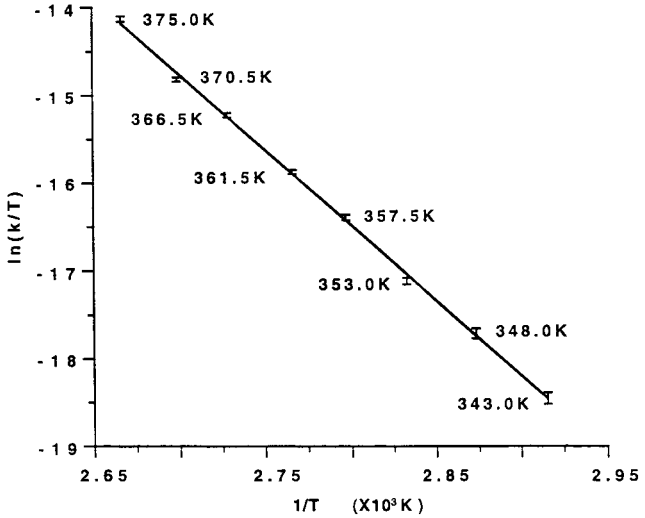

Figure 8. Eyring plot for the *endo* to *exo* isomerization of $Os(PMe_2Ph)_3(\eta^4$-*o*-$C_6Me_4(CH_2)_2\}$ (**3**).

a constant, limiting value in the presence of >4 mmol of PMe_3. A similar but less pronounced effect is evident for the isomerization of the osmium−PMe_2Ph complex, *endo*-**3**, in the presence of added PMe_2Ph (Figure 10). In contrast, the rate of disappearance of the osmium−PMe_3 complex, *endo*-**2**, is almost independent of added PMe_3 (Figure 11).

For *endo*-**1** and *endo*-**3**, the observations are consistent with the hypothesis that isomerization occurs by two pathways, one of which requires initial dissociation of tertiary phosphine while the other does not. A plausible, tractable model for the process is shown in Scheme 2. In the dissociative process, a reversible preequilibrium generates the 16-electron intermediate $ML_2\{\eta^4$-*endo*-Me_4-*o*-xylylene} (B) by dissociation of tertiary phosphine (L) from the *endo*-ML_3 complex (A), with rate constants k_1 and k_{-1} for the forward and reverse reactions. The ML_2 fragment in B migrates irreversibly from the *endo* to the *exo* pair of double bonds with the rate constant k_2, generating the second intermediate $ML_2\{\eta^4$-*exo*-Me_4-*o*-xylylene} (C), which picks up L rapidly and irreversibly with a rate constant k_3 to form the *exo*-ML_3 complex (D). In the nondissociative process,

Table 9. Activation Parameters for *endo* to *exo* Isomerization of $ML_3\{\eta^4\text{-}o\text{-}C_6Me_4(CH_2)_2\}$ (M = Ru, L = PMe_3 (1); M = Os, L = PMe_3 (2); M = Os, L = PMe_2Ph (3))

process	$\Delta H^{\ddagger}$ (kJ mol^{-1})	$\Delta S^{\ddagger}$ (J mol^{-1} K^{-1})	E_{act} (kJ mol^{-1})	ln *A*
endo-**1** → *exo*-**1**[a]	103.9(0.7)	−36.0(2.0)	106.8(0.7)	26.3(0.2)
endo-**2** → *exo*-**2**[a]	147.8(1.8)	+67.2(4.8)	153.6(1.8)	38.8(0.6)
endo-**3** → *exo*-**3**[a]	168.1(1.7)	+141.5(4.8)	171.1(1.7)	47.7(0.6)
endo-**1** → *exo*-**1** (dissoc pathway)[b]	123.3(3.9)	+12.5(10.5)	126.3(3.9)	32.2(1.3)
endo-**1** → *exo*-**1** (direct pathway)[c]	105.6(1.6)	−36.9(4.9)	108.6(1.8)	26.2(0.5)
endo-**2** → **8**[c]	107.4(1.8)	−42.4(4.9)	110.5(1.8)	25.6(0.6)
endo-**1** → **9**[c]	142.9(1.5)	+65.4(4.1)	199.7(7.0)	56.3(2.5)

[a] In the absence of added L. [b] Rate data obtained by subtraction of observed rate in the presence of an excess of L (20 equiv) from that in the absence of added L. [c] Rate data in the presence of an excess of L (20 equiv).

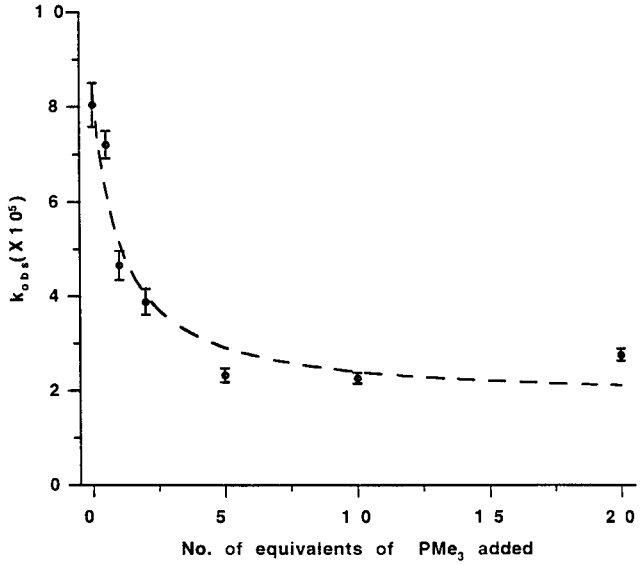

Figure 9. Dependence of k_{obs} on added PMe_3 for the *endo* to *exo* isomerization of $Ru(PMe_3)_3\{\eta^4\text{-}o\text{-}C_6Me_4(CH_2)_2\}$ (**1**) at 357.5 K. The dotted line represents the calculated curve (see text).

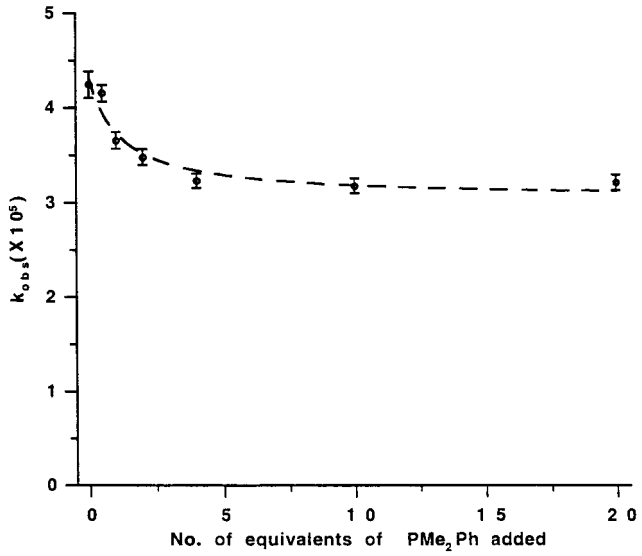

Figure 10. Dependence of k_{obs} on added PMe_2Ph for the *endo* to *exo* isomerization of $Os(PMe_2Ph)_3\{\eta^4\text{-}o\text{-}C_6Me_4\text{-}(CH_2)_2\}$ (**3**) at 357.5 K. The dotted line represents the calculated curve (see text).

A isomerizes directly to D with the rate constant k_5; this process is assumed to be irreversible. In the case of osmium, complex D is in equilibrium with added L and

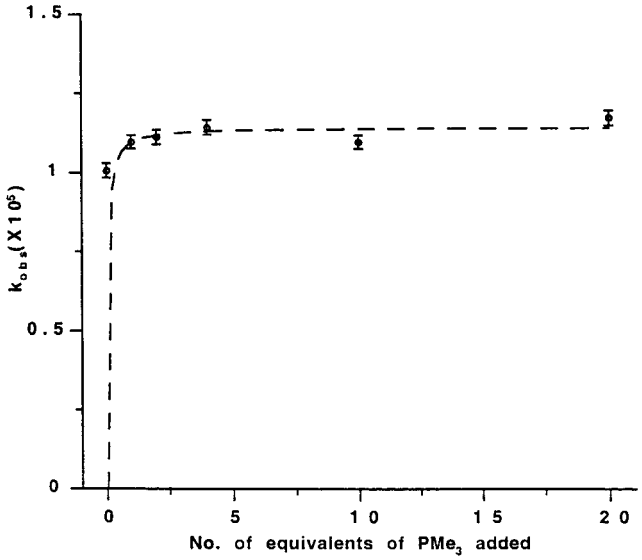

Figure 11. Dependence of k_{obs} on added PMe_3 for the *endo* to *exo* isomerization of $Os(PMe_3)_3\{\eta^4\text{-}o\text{-}C_6Me_4(CH_2)_2\}$ (**2**) at 379.5 K. The dotted line represents the calculated curve (see text).

Scheme 2

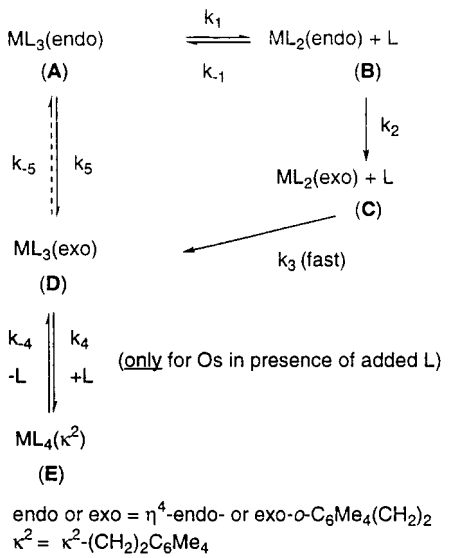

$OsL_4\{\kappa^2\text{-}Me_4\text{-}o\text{-xylylene}\}$ (E), the forward and reverse rate constants being k_4 and k_{-4}.

Application of the steady-state approximation (SSA) to the concentration of B yields eqs 7 and 8. If L is small or changes slowly with time, this corresponds with the observed first-order behavior (eq 9). Clearly, $k_{obs} = k_1 + k_5$ when [L] = 0 and $k_{obs} = k_5$ when L→ ∞.

The validity of the SSA model has been checked by

$$[B] = \frac{k_1[A]}{k_2 + k_{-1}[L]} \quad (7)$$

$$\frac{d[A]}{dt} = -(k_1 + k_5)[A] + k_{-1}[B][L] \quad (8)$$

$$\frac{d[A]}{dt} = -k_{obs}[A] \quad (9)$$

$$k_{obs} = k_5 + k_1\left\{\frac{1}{1 + k_{-1}[L]/k_2}\right\} \quad (10)$$

numerical simulations (see Experimental Section and Supporting Information), which show that, for the *endo* to *exo* isomerization of **1** and **3**, the rate constant k_{obs} and the extracted kinetic parameters are insensitive to the formation of the κ^2 complex E. We have therefore used the SSA model to extract kinetic parameters from the experimental data for **1** and **3** by iterative curve fitting to eq 10. The calculated curves are compared with the experimental data in Figures 9 and 10. The derived kinetic parameters at 357.5 K are $k_1 = (6.56 \pm 0.86) \times 10^{-5}$ s^{-1}, $k_5 = (1.78 \pm 0.62) \times 10^{-5}$ s^{-1}, and $k_{-1}/k_2 = 0.95 \pm 0.44$ equiv^{-1} (regression coefficient 0.968) for **1**, $k_1 = (1.27 \pm 0.17) \times 10^{-5}$ s^{-1}, $k_5 = (3.04 \pm 0.13) \times 10^{-5}$ s^{-1}, and $k_{-1}/k_2 = 0.83 \pm 0.39$ equiv^{-1} (regression coefficient 0.967) for **3**.

It seems likely that the reversible dissociative process plays little if any role in the isomerization of *endo*-**2,** in view of the lack of dependence of the rate on PMe_3 concentration. In this case, therefore, we consider only the following processes occurring in nondissociative isomerization:

$$A \underset{k_{-5}}{\overset{k_5}{\rightleftharpoons}} D$$

$$D + L \xrightarrow{k_4} E \ (L = PMe_3)$$

Applying the SSA to the concentration of D and assuming (1) that the concentration of L is small or changing only slowly with time and (2) that the steady-state concentration of L is near its initial value, we obtain eqs 11 and 12. The following values allowed a reason-

$$\frac{d[A]}{dt} = -k_{obs}[A] \quad (11)$$

$$k_{obs} = \frac{k_5}{1 + k_{-5}/k_4[L]} \quad (12)$$

able representation of the results at 379.5 K: $k_5 = 1.14 \times 10^{-4}$ s^{-1}, $k_{-5} = 0.049 \times 10^{-4}$ s^{-1}, and $k_4 = 0.59 \times 10^{-4}$ s^{-1} equiv^{-1}. The concentration profiles show, not surprisingly, that the SSA is poor for [L] = 0, 1, or 2 equiv per equiv of [A], so these values must be treated with caution.

Discussion

The observations reported here extend earlier work on *o*-xylylene complexes in two respects. First, although the *endo* and *exo* isomers of η^4-*o*-xylylene with $Ru(PMe_2Ph)_3$ had been characterized,[11,12] these did not interconvert in solution under normal conditions; hence, it was not possible to verify experimentally the theoretical prediction of the greater stability for the *exo* isomer.[16] The presence of methyl substituents at the 3−6-positions of the *o*-xylylene lowers the barrier to the *endo* to *exo* isomerization to such an extent that (a) $Ru(PMe_2Ph)_3\{\eta^4$-*endo*-*o*-$C_6Me_4(CH_2)_2\}$ (*endo*-**7**) cannot be isolated or detected and (b) the kinetics of the isomerization can be studied in an experimentally readily accessible temperature range for $ML_3\{\eta^4$-*o*-$C_6Me_4(CH_2)_2\}$ (L = PMe_3, M = Ru (**1**), Os (**2**); L = PMe_2Ph, M = Os (**3**)). These effects can probably be traced in part to a ground-state destabilization of the *endo* isomer. Comparison of the bond lengths of $Os(PMe_2Ph)_3\{\eta^4$-*endo*-*o*-$C_6R_4(CH_2)_2\}$ (R = H, Me) shows that the four methyl groups in **3** cause a significant lengthening of the Os−C bonds, presumably weakening the Os−diene interaction. The effect is similar to that observed in metal−alkene complexes and may be ascribed to a combination of steric hindrance and weakening of metal−alkene back-bonding resulting from the electron-donating effect of the methyl groups.[46,47]

In contrast to their ruthenium(0) analogues, the η^4-*exo*-*o*-xylylene complexes of osmium(0), *exo*-**2** and *exo*-**3**, take up an additional molecule of tertiary phosphine (reversibly for **3** and PMe_2Ph, irreversibly for **2** and PMe_3) to give the κ^2 complexes **8** and **9**. The density functional calculations reproduce the greater stability of the κ^2 complexes for the heavier element, which probably reflects the greater stability of metal−carbon σ-bonds for 5d relative to 4d elements,[48,49] but they predict incorrectly that the κ^2 complexes should be the stable species in the presence of an excess of ligand for both metals. The most likely source of systematic error lies in an overestimate of the strength of the M−P bonds. This will not affect the comparison of the relative energies of the *endo* and *exo* isomers, but it will be significant in comparing ML_4 with ML_3 complexes. Moreover, steric interactions are likely to be greater in the ML_4 complexes, so that the calculations will tend to overestimate the stability of ML_4 relative to ML_3. Clearly, the common device of replacing PR_3 by PH_3 in order to simplify computations is misleading in this case. The marked differences resulting from replacement of PMe_2Ph by PMe_3, which are likely to be of largely steric origin, are evident in the chemistry reported here.

The *endo*- to *exo*-isomerizations of complexes **1** − **3** are examples of haptotropic rearrangements, in which a metal−ligand fragment, such as $M(CO)_3$, migrates between coordinated and uncoordinated C=C bonds.[50] In some cases the processes occur at rates on the NMR time scale,[51,52] but the examples reported here are more

(46) Yamamoto, A. *Organotransition Metal Chemistry, Fundamental Concepts and Applications*; Wiley-Interscience: New York, 1986; pp 212−222.
(47) Pruchnik, F. P. *Organometallic Chemistry of the Transition Elements*; Plenum: New York, 1990; pp 343−346.
(48) Reference 46, pp 47−51.
(49) Reference 47, p 201.
(50) Albright, T. A.; Hofmann, P.; Hoffmann, R.; Lillya, C. P.; Dobosh, P. A. *J. Am. Chem. Soc.* **1983**, *105*, 3396 and references therein.
(51) Mann, B. E. In *Comprehensive Organometallic Chemistry*; Wilkinson, G., Stone, F. G. A., Abel, E. W., Eds.; Pergamon: Oxford, U.K., 1982; Vol. 3, p 90.
(52) Mann, B. E. *Chem. Soc. Rev.* **1986**, *15*, 167.

akin energetically to the 1,3-rearrangements in $Fe(CO)_3$ complexes of η^4-1,3,5-cycloheptatriene and substituted cycloheptatrienes,[53,54] acyclic polyene iron tricarbonyls (e.g., that shown in eq 13),[55−61] and $Cr(CO)_3$ complexes of η^6-naphthalene and substituted naphthalenes (eq 14).[62,63] For the iron tricarbonyls, the rearrangements

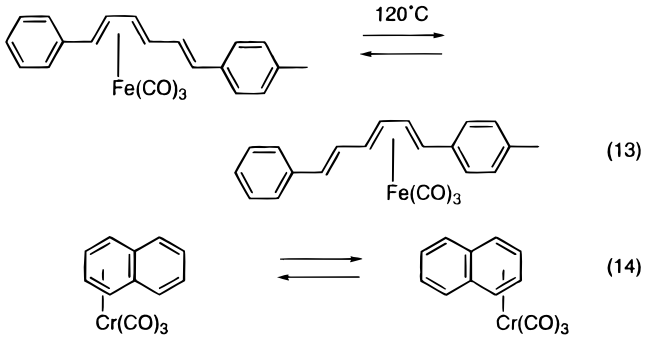

(13)

(14)

are believed to occur via a 16-electron intermediate or transition state $Fe(CO)_3(\eta^2$-polyene), although a pathway proceeding via a dicarbonyl, $Fe(CO)_2(\eta^4$-polyene), seems to have been explicitly eliminated only in the case of the substituted cycloheptatriene complexes $Fe(CO)_3$-(η^4-*exo*- C_7H_7R) (R = Me_3Si, Me_3Ge, Ph_3Ge).[54] Theoretical calculations[50] on the mechanism of the degenerate $\eta^6 \rightarrow \eta^6$ rearrangement of $Cr(CO)_3(\eta^6$-$C_{10}H_8)$ support a circuitous pathway in which naphthalene undergoes partial dissociation to a η^2-exocyclic intermediate.

As expected, in the *endo* to *exo* isomerization of **1** and **3**, the ligand-dependent dissociative pathway plays a more significant role for the bulkier ligand PMe_2Ph than for PMe_3 and, perhaps less predictably, for ruthenium compared with osmium. However, the activation parameters listed in Table 9 do not seem to be amenable to any simple interpretation. The E_a and $\Delta H^{\ddagger}$ values for the *endo* to *exo* isomerization of **1** are smaller than those for **2** and **3**, consistent with the stronger metal−ligand bonds and lower lability of 5d-element complexes relative to their 4d-element analogues. The small, positive activation entropy $\Delta S^{\ddagger}$ for the dissociative pathway in the isomerization of *endo*-**1** is also as expected for this type of process.[64−66] However, the value of $\Delta S^{\ddagger}$ for the net process, in the absence of PMe_3, is negative, even though ca. 75% of the isomerization proceeds by the dissociative route. Even more surprising are the large positive values of $\Delta S^{\ddagger}$ for the isomerization of *endo*-**2** in the absence of added PMe_3 and *endo*-**3** in the absence of added PMe_2Ph, where the route depending on dissociation of L appears to play little role (in the case of **3**, ca. 25%) or no role. The results may indicate that aromatic solvent plays a specific role in the isomerizations of the *endo* osmium complexes.

At this stage, one can only speculate about intermediates or transition states. For the ligand-independent process, a concerted loosening of one of the *endo* double bonds via species **10** seems plausible. Loss of a ligand

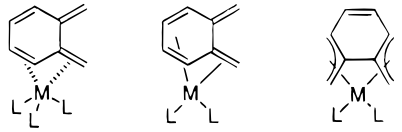

10 **11** **12**

L could generate formally 18-electron ML_2 complexes having structures such as **11** or **12**; current research is directed to the possible stabilization of such intermediates by use of sterically bulky tertiary phosphines.

Acknowledgment. We thank Johnson-Matthey Co., Royston, U.K., for a loan of hydrated ruthenium(III) chloride, and Professors Denis Evans and Alan Sargeson for helpful discussions.

Supporting Information Available: Tables giving crystallographic data, atomic coordinates and equivalent isotropic displacement parameters, anisotropic displacement parameters, interatomic distances and angles for non-hydrogen atoms, interatomic distances, angles, and torsion angles for hydrogen atoms, and selected least-squares planes for *endo*-**3**, *exo*-**3**, *exo*-**1**, and **8** and text and tables giving details of the kinetics simulation (134 pages). Ordering information is given on any current masthead page.

OM9804226

(53) Karel, K. J.; Albright, T. A.; Brookhart, M. *Organometallics* **1982**, *1*, 419.
(54) LiShingMan, L. K. K.; Reuvers, J. G. A.; Takats, J.; Deganello, G. *Organometallics* **1983**, *2*, 28.
(55) Whitlock, H. W.; Chuah, Y. N. *J. Am. Chem. Soc.* **1965**, *87*, 3605.
(56) Whitlock, H. W.; Reich, C. D.; Woessner, W. D. *J. Am. Chem. Soc.* **1971**, *93*, 2483.
(57) Whitlock, H. W.; Markezich, R. L. *J. Am. Chem. Soc.* **1971**, *93*, 5290.
(58) Whitlock, H. W.; Markezich, R. L. *J. Am. Chem. Soc.* **1971**, *93*, 5291.
(59) Goldschmidt, Z.; Bakal, Y. *J. Organomet. Chem.* **1984**, *269*, 191.
(60) Hafner, A.; von Philipsborn, W.; Salzer, A. *Angew. Chem., Int. Ed. Engl.* **1985**, *24*, 126.
(61) Goldschmidt, Z.; Hezroni, D.; Gottlieb, H. E.; Antebi, S. *J. Organomet. Chem.* **1989**, *373*, 235.
(62) Kündig, E. P.; Desobry, V.; Grivet, C.; Rudolph, B.; Spichiger, S. *Organometallics* **1987**, *6*, 1173.
(63) Oprunenko, Y. T.; Malyugina, S. G.; Ustynyuk, Y. A.; Ustynyuk, N. A.; Kravtsov, D. N. *J. Organomet. Chem.* **1988**, *338*, 357 and references therein.
(64) Atwood, J. D. *Inorganic and Organometallic Reaction Mechanisms*, 2nd ed.; VCH: Weinheim, Germany, 1997; p 14.
(65) Mann, B. E.; Musco, A. *J. Chem. Soc., Dalton Trans.* **1980**, 726.
(66) Krassowski, D. W.; Nelson, J. H.; Brower, K. R.; Hauenstein, D.; Jacobson, R. A. *Inorg. Chem.* **1988**, *27*, 4294.